Supplementary Materials for

Organic matter preserved in 3-billion-year-old mudstones at Gale crater, Mars

Jennifer L. Eigenbrode,* Roger E. Summons, Andrew Steele, Caroline Freissinet, Maëva Millan, Rafael Navarro-González, Brad Sutter, Amy C. McAdam, Heather B. Franz, Daniel P. Glavin, Paul D. Archer Jr., Paul R. Mahaffy, Pamela G. Conrad, Joel A. Hurowitz, John P. Grotzinger, Sanjeev Gupta, Doug W. Ming, Dawn Y. Sumner, Cyril Szopa, Charles Malespin, Arnaud Buch, Patrice Coll

*Corresponding author. Email: jennifer.l.eigenbrode@nasa.gov

This PDF file includes:

Materials and Methods
Supplementary Text
Figs. S1 to S11
Tables S1 to S10
References

Materials and Methods

Samples and Geological Context

Samples are from three key locations: Yellowknife Bay, Pahrump Hills and Marais Pass. They comprise the Sheepbed member of the Yellowknife Bay formation and the Murray formation for the two other localities. All of the samples have similar lithology dominated by parallel, finely laminated mudstones deposited in an ancient deltaic-lacustrine setting (*6, 30*). The lacustrine environments like that interpreted for Gale lake(s) strongly support the concentration, preservation, and potential formation (by microbiology) of organic matter as they do on Earth (*9*).

Details of the stratigraphy and geological context are presented elsewhere (*3, 6-8, 30*). In brief, John Klein (JK) and Cumberland (CB) drill targets are located in Yellowknife Bay. Yellowknife Bay occurs in the lowest point along the rover traverse (-4520 m elevation) which resides in a broad valley between the crater rim and central mound of Gale crater. This mudstone is thought to contain sediments transported by fluvial and deltaic processes from the crater rim area to the north (*30*). They are stratigraphically within ≈10 cm apart, laterally about 3 m apart and differ in their diagenetic state, such that JK contains calcium sulfate-filled concretions and veins, while CB was observed to be largely vein-free (*29*). The veins and concretions likely indicate post-depositional diagenesis by groundwater (*34*). Pahrump Hills and Marais Pass are drill targets in the Murray formation of the lowermost portion of the Gale Crater central mound located about 6-7 km southwest of Yellowknife Bay. The Pahrump Hills samples Confidence Hills (CH sample at -4460 m elevation) is at the base followed by drill target Mojave 2 (MJ at -4461 m; number designates the second drill hole), and Telegraph Peak (TP at -4453 m). Buckskin (BK at -4447 m) occurs higher in the Marias Pass region.

Mineralogy of the mudstone samples consistently exhibits basaltic components (i.e., feldspar and mafic igneous minerals); however, in bulk composition they show significant differences (*7*). The Sheepbed mudstone contains iron oxides/hydroxides, traces of iron sulfides (~1% by mass pyrrhotite in JK and CB, and perhaps 0.3% pyrite in JK), a Si/Fe/S-rich amorphous phase (~30%) (*28, 35*), and authigenic Fe-smectite (~20%), which was probably formed by reaction of magnetite and olivine under circumneutral pH conditions (*36*). Oxychlorine phases detected by SAM EGA and CheMin instruments are likely composed of perchlorate/chlorate and akaganeite (*2, 3*). The oxygen evolved from the perchlorate is responsible for combustion of SAM background and possibly some sample organics (*2*).

At Pahrump Hills/Marais Pass, the Murray mudstones mineralogy exhibits 27-54% x-ray amorphous material composed largely of silica (*5*). The CH and MJ targets exhibits dendrites and crystal laths of probable magnesium sulfate composition (*6, 37*). The CH and MJ samples also host phyllosilicates (5-8%) of unknown origin and lesser amounts of jarosite and apatite (*7*). Magnetite abundance increases upsection but returns to low amounts at Marais Pass (BK target) and hematite consistently decreases upsection CH through BK samples. The top of this section (TP and BK) is unique in that it contains a high abundance of crystalline silica minerals: cristobalite and tridymite. The CH, MJ, TP, and BK samples also contain an oxychlorine phase that generates an O_2 release below 500°C. CH, MJ, and TP samples show a second higher temperature O_2 release that is attributed to sulfate decomposition (*3*). Similar to the JK and CB samples, the presence of evolved O_2 can complicate detection of organic molecules. Iron sulfides were not detected by the CheMin X-ray diffractometer in the lower Murray formation (*7*).

The mineralogy and sedimentological features of the Yellowknife Bay and lowermost Murray formations suggest a complex geochemical history for the evolving Gale lake environment. Various hypotheses for lake conditions during Yellowknife Bay and early Murray deposition and subsequent aqueous events have been reported (*7, 8, 32*). It is likely that both surface fluvial water and groundwater fed the lake basin. The lake surface environment may have been relatively oxidizing due to ultraviolet radiation and oxidizing surface chemicals compared to more reducing, ferrous-iron bearing groundwater feeding the lake (*8*). Groundwater may have also delivered sulfides from hydrothermal sources (*32*). Lake water was probably circumneutral pH or alkaline; however, during diagenesis acidic fluids may have passed through the lower Murray formation (*7, 34*).

SAM experimental methods

The SAM Evolved Gas Analysis/Gas Chromatography Mass Spectrometry (EGA/GCMS) experiments described in the main text are for analysis of solid samples. Each sample was collected by a rotary-percussive drill from a depth of 1-5 centimeters from the rock surface and then was passed through a 150-μm sieve in the Collection and Handling for In-Situ Martian Rock Analysis (*38*) before delivery of the <150-μm sized fraction to SAM via the Solid Sample Inlet Tube (SSIT). For each set of EGA/GCMS experiments, before samples were received by SAM, an empty quartz cup was placed in the oven and heated to ~900°C, a process referred to as preconditioning. The cup design allows pure helium (99.999%) to flow through a frit at the bottom of the sample reservoir and the outside of the cup to sweep analytes to the manifold. The pressure in the oven is held constant pressure at ~ 25 mbar and flows at 0.03 bar-ml/sec (equivalent to ~0.77 standard cm^3 per minute). Helium is introduced through a flow restrictor was flushed through the oven and 135°C-heated manifolds, traps, GC, and then to the vent to condition the instrument suite for analysis (*10, 39*). No mass spectral data was collected by the quadrupole mass spectrometer (QMS) to conserve resources. On a subsequent sol, one or multiple portions of drill fines were then deposited into a quartz glass cup within the Sample Manipulation System (SMS) of SAM. Based on estimates of the portion volume and powder density from MSL's Sample Acquisition, Sample Processing, and Handling testbed (*38*) experiments, models using geological materials with similar properties, and drop tests of a drilled mudstone in MSL testbeds at the Jet Propulsion Laboratory, each SAM portion is estimated to be 45 ± 18 mg (2σ standard deviation). Each aliquot of sample delivered to SAM is designated *target name-#* (e.g., Mojave 2-1 is the Mojave 2 drill target, first aliquot delivered to SAM but herein referred to as MJ for brevity).

For analysis, the samples were heated under the same helium flow from an initial temperature (35°-50°C, unless noted as a preheat temperature in Table S6) at nominal rate of 35° C/min; however, the heating rate is significantly reduced once the sample temperature exceeds ~750° C and the heater output is maximized. During heating, organic molecules evolve from larger organic components and minerals via several mechanisms: thermal desorption (volatilization), pyrolysis (cleavage), or thermochemical reactions (e.g., hydrolysis induced by the presence of water during pyrolysis). In some cases, minerals that occlude organics at grain boundaries or within mineral crystals must first thermally decompose or decrepitate to allow organic materials to evolve. Inorganic chemicals also undergo chemical reactions; thus, heating induces an ongoing complex reaction chemistry. The efficiency of extraction of organic components is dependent on instrument conditions and sample chemistry.

For EGA, gases were sent through a short manifold and then passed by a capillary inlet to the QMS. The fixed capillary conductance is sized to keep the MS in a safe operating range while still admitting sufficient gas to realize good sensitivity and dynamic range in the QMS signal. The QMS scanned the 2-535 Da range for EGA characterization of bulk gases.

Only 0.125% of the gas flowing through the manifold enters the QMS for EGA. The remainder is sent to the GC, tunable laser spectrometer, or a vent. Gases sent to the GC represent the portion evolved over a select temperature range (called the GC cut) (Table S2). This portion is first passed over the cooled hydrocarbon adsorption trap and then thermally released to the GC injection trap (*1, 10*).

Following the EGA part of the EGA/GCMS experiment, the manifold is pressurized to nearly 1 bar and a flow of gas is established through one or more GC columns. Gas is thermally released from the hydrocarbon trap and the less volatile component is trapped on an injection trap in front of the GC column. After the column has been conditioned by flowing the carrier gas through the column and the QMS has been turned on, the gas trapped on the injection trap is rapidly released by heating and held for several seconds. The injection trap focuses the analytes in a narrow band at the front of the column to achieve sufficiently narrow elution peaks for MS analysis. For all the GCMS experiments described here, the column used was a wall-coated open tubular column with a phenyl- and cyanopropyl-polydimethylsiloxane film. The column that targets organic compounds in the C5-C15 molecular weight range is designated GC5. More details of the GC oven and MS parameters are reported elsewhere (*1, 2*). GCMS analyses were conducted on all solid samples except Telegraph Peak, for which only the EGA portion was implemented, and Buckskin, for which the GC portion of the experiment did not complete.

The sample mass and the temperature cuts selected for the GCMS analysis are given in Table S2 and S6. In the EGA part of the Mojave experiment, sufficient material was apparently released to temporarily clog the injection trap. This was established by examining diagnostic data from pressure sensors and the signal from the QMS, which showed a backflow of atmospheric gas that would not have been present with the nominal flow through the GC column. Diagnostic experiments that introduced a pulse of helium gas into the manifold cleared the flow path through the injection trap, and since most of the gases evolved from Mojave were still trapped, a successful GCMS run was subsequently implemented. As a result of this off-nominal GC run, some compounds show a 20 s shift in retention time.

Blank tests were conducted on preconditioned, empty cups prior to initial sample delivery at each site and were run under the same conditions as the first sample with the intent of providing a gauge for background signal strength and the presence of "sticky" volatiles from sample-to-sample carryover, such as SO_2 and HCl. During blank experiments, the empty cup is exposed to the SMS and SSIT in the same manner as sample delivery.

A modified sample delivery approach was used for CB6, CB6-reheat, CB7 and CB blank2 tests in an attempt to reduce the amount of SAM instrument background. This modified approach entailed He-flushing and pumping of the SMS for 360 min and venting SMS volatiles to the atmosphere. During this time, the SAM manifold was heated to 135° C and the oven was flushed with He. In addition, the sample cup was heated in the oven for 20 minutes to either 200° or 249°C (Table S6) before moving the cup to the SSIT for sample delivery. During hot-cup transfer, the cup and contents (if any) cool to an unknown extent. For triple portion samples (CB6 and CB7), cup heating was done before each of the three separate portions, such that some of the sample was heated to 249° C and the volatiles vented to atmosphere without detection. During CB6 reheat analysis (i.e., rerun of the residue remaining after the first analysis) and CB blank2 tests, the cup

was processed in the same manner as CB6 and CB7, mimicking the motions of three sample portion deliveries (without actual delivery) so that SMS exposure would be comparable to the triple portion samples.

SAM GC breadboard tests for confirmation of organic-sulfur compounds and naphthalene

The retention times of the organic sulfur molecules were determined using a laboratory ThermoFisher Scientific UltraTrace GC coupled to an ITQ mass spectrometer and run with SAM-like analytical conditions (column temperature and the carrier gas pressure and flow). Laboratory results offer a direct comparison to the retention time of molecules observed on the SAM flight model on Mars (Table S3). The GC column was a duplicate of the SAM GC5 column. Retention times for compounds (e.g. naphthalene) eluting from the column at high temperatures, i.e., after the second injection trap flash heating, are challenging to replicate for the flight SAM instrument and retention times are not precise. Consequently, the possible EGA naphthalene detection for Mojave could not be precisely confirmed on the SAM GC breadboard. Benzothiophene does not elute from the GC5 column operated under SAM conditions.

Characterization of the SAM instrument background in EGA

A diverse set of masses in the bulk gas were released up to 350º to 550ºC (depending on the sample) that reflect both thermal desorption and pyrolysis largely attributable to reaction products of the derivatization fluid composed of N-*tert*-butyldimethylsilyl-N-methyltrifluoroacetamide (MTBSTFA) and dimethylformamide (DMF). This fluid leaked into the sample manipulation system after a foil-seal failed (40). Consequently, the reagents adsorb onto cup and sample surfaces, as cups are moved between oven and sample receiving position. For this reason, only EGA signals for the high temperature range (>400º or >550ºC depending on sample) are closely examined. Furthermore, contributions from known and suspected residual derivatization reaction products that evolve at high temperatures are subtracted from the raw data. Mass channels of interest were corrected for inputs from specific products and for trending background signals. This dual approach enables robust examination of the SAM EGA data for mudstone-derived signals.

Characterization of SAM instrument background in EGA derived from derivatization reagents

Understanding the nature and significance of the observed organic signatures in analyses of martian samples requires evaluation of the gases evolved over the full thermal range and a comprehensive, reproducible approach to distinguishing background from sample-derived organics. Organic molecules in the SAM instrument background are largely derived from the 4:1 (volume/volume) solution of N-methyl-N-(*tert*-butyldimethylsilyl)-trifluoroacetamide (MTBSTFA; $C_9H_{18}F_3NOSi$) and dimethylformamide (DMF; C_3H_7NO) reagent (1, 40) stored in seven sealed cups within the SAM SMS to support the SAM derivatization experiment (10). No derivatization cups have been punctured as of the Pahrump Hills investigation, but the presence of reaction products in all martian analyses indicates a cup is leaking derivatization vapors into the SMS where they can be adsorbed and react with water, quartz glass cups and sample in the SMS (1, 40).

In EGA, SAM background signals change in character during heating from 45° to 860°C. DMF is a solvent and proton acceptor for MTBSTFA and its presence has not been observed in SAM EGA or GCMS analyses. MTBSTFA is a silylating reagent that that replaces active hydrogen atoms of polar functional groups (alcohol hydroxyl, phenol hydroxyl, carboxyl, amine, and amide). The reaction involves nucleophilic attack by the analyte heteroatom (O, N, Cl, or F) on the Si atom of the silylation reagent and forms *tert*-butyldimethylsilyl (TBDMS) derivatives (usually as TBDMS ethers [$(CH_3)_3CSi(CH_3)_2$-O-R)] as intended for the experiment) and the byproduct: 2,2,2-trifluoro-N-methyl-acetamide (TFMA; $C_3H_4F_3NO$). It also preferentially reacts with water vapor and hydrated minerals, HCl, and OH-sites on mineral surfaces (*41, 42*). Reaction products are both volatile and non-volatile. Both volatile products and derivatized mineral surfaces can undergo pyrolysis (thermal cracking involving covalent bond cleavage). They are also susceptible to combustion in the presence of O_2 released from the samples (*2, 41, 42, 43, 44*). Combustion occurs in all samples due to the presence of oxychlorine phases and in some samples, other unknown chemicals. The MTBSTFA reagent in its most pure commercially available form is only ≥97% determined by GC and thus some of the signals observed in EGA at low temperatures may be directly volatilized impurities and the impurities would also be susceptible to combustion.

Consequently, a suite of molecular products characterizes the SAM instrument background (Table S5). Most products are released below 550°C in the presence of martian sediments (400°C for Yellowknife Bay mudstones) (Fig. S7). Both SAM solid sample analyses and laboratory analyses indicate that the inorganic sample chemistry (e.g., oxychlorine phases, other reactive phases, and mineral catalysts) has a significant effect on the temperature and character of MTBSTFA reaction products released. In blanks, products are released more continuously into >550°C temperature range, which is comparable to laboratory silylation experiments of ashed fused silica. Pyrolysis of TBDMS-minerals generates C1-C4 aliphatic compounds, particularly methane and methylpropene. This pyrolytic release reaches its maximum after the thermal desorption of volatile products and within the 400°-750°C window.

After the bulk of the SAM instrument background volatiles are released below 550°C, a steady but low level of the molecules persists into higher temperatures (Fig. S11). This portion is referred to as the tailing of the main release peak in any mass channel and is the portion of signal removed during data processing to resolve the presence or absence of sample-related organic volatiles (see below). SAM EGA experiments occur at ~0.03 bar-ml/min helium flow (*10*) to conserve helium gas, which is a limited resource on the multiyear Mars mission. The SAM EGA flow condition differ from traditional laboratory thermal experiments conducted at ≥20 bar-ml/min in the pyrolysis oven. The difference in volumetric flow and different pressures results in several hundred times more mass flow in traditional lab analyses compared to SAM experiments on Mars. Lower mass flow in the oven is likely responsible for peak broadening and tailing of some analytes.

Based on SAM and laboratory analyses, the MTBSTFA reaction and pyrolysis products in Table S5 have been observed. Halogenated organic molecules are observed when inorganic halogen-containing species are present. Some molecules in the SAM instrument background include ions in their mass spectra with masses the same as those that are most diagnostic for some organic sulfur and aromatic compounds. For each potential conflict in molecular source assignments, tests were implemented to estimate the relative portion of the mass signal from background. Further, there are no known MTBSTFA-related contributions to *m/z* 112; thus, these likely reflect another source of organic carbon (*1*).

Characterization of SAM instrument background in EGA from PTFE-contaminant delivery to SAM

The only known organic contaminant external to SAM is polytetrafluoroethylene (PTFE, trademarked as Teflon by DuPont, Inc.) debris physically abraded from a seal in the drill bit assembly. Samples are delivered to SAM via Curiosity's drill and CHIMRA systems. Pyrolysis of PTFE has been well characterized (*45*) and it is responsible for a reproducible *m/z* 81 and 100 peak observed as a discrete peak at ~550°C in some SAM analysis of drilled sample (Fig. S8), though of varying magnitude. Lab analyses demonstrate that PTFE pyrolysis products are not aromatic in nature and appear to be relatively non-reactive. Thus, PTFE does not contribute to any of the signals assigned to organic sulfur or aromatic compounds and is unlikely to be related to aliphatic compounds observed at higher temperatures in samples.

Besides PTFE, the only other potential and suspect contaminants would be polyimide from tape (trademarked as Kapton by DuPont, Inc.) and phthalate plasticizers ubiquitous in terrestrial airborne particulates. If by remote chance these contaminants entered the SAM quartz cups for pyrolysis, polyimide would have produced a very wide variety of aromatic compounds that should be readily detectable by SAM in both EGA and GC and they would evolve over the entire 500-860°C range (*46*). The results observed for drilled samples by SAM are inconsistent.

Phthalate esters thermally decompose at ~425°C and their products are largely functionalized single-ring aromatic moieties that are expected to produce chlorobenzene (*47*) in the presence of HCl gas. Martian samples show HCl gas release into high temperatures (*3*). If this scenario had occurred, then chlorobenzene should have been observed in the four Rocknest series of analyses. Chlorobenzene was not observed in Rocknest. Since phthalate particles are not expected from the martian environment or from delivery via the drill and CHIMRA systems, particularly after multiple uses, and the temperature of pyrolysis is inconsistent with all observed occurrences of chlorobenzene and other masses suggestive of aromatics, it is highly unlikely that terrestrial phthalates are the source of aromatic compounds in the SAM analyses.

Characterization of the SAM instrument background in GC

Additional components contribute to the SAM internal background for GC analyses. These are the hydrocarbon trap that contains Tenax TA adsorbent and the injection trap to the GC5 column that contains Tenax GR. Both are made of 2,6-diphenyl-p-phenylene oxide that undergoes thermal and chemical degradation with use and releases aromatic compounds and perhaps aliphatic compounds. Miller et al. (*47*) and Freissinet et al. (*1*) review details of Tenax degradation products and their implications.

Importantly, several valves present in the flow path between the He tanks, oven and the gas-line manifold with the hydrocarbon trap prevent backflow of Tenax degradation products to the portion of the instrument used for EGA (see Figure 3 of Freissinet et al. (*1*)). When the valves are open, helium flows away from the EGA portion and flushes the traps and GC portion to a vent. Furthermore, the 135°C-heated manifolds are sufficiently warm to volatilize GC/trap derived background organic molecules, which would be flushed from the gas lines during the preparation and preheat stages of each experiment and could not produce peaks in EGA profiles. GC/trap-derived background organic molecules are not contributing to EGA signals.

Data Processing: EGA mass channel corrections for volatile contributions from background organic molecules

EGA mass channel data (or m/z profiles) were corrected for known or assumed ion contributions from other volatiles. All or part of the experimental temperature range was corrected. The objective of the corrections was to calculate a m/z profile that more accurately reflects the evolution of particular volatiles and their abundances.

Relative molar response (RMR) of mass fragment intensities were determined based on the mass spectra for one or multiple volatile contributions to be removed. The RMR calculated for each volatile to be removed was equivalent to the intensity ($I_{spectrum}$) of the diagnostic m/z for the volatile of interest (X) relative to that of the diagnostic m/z for volatile contribution to be removed (Y) (Eq. 1). Published NIST mass spectra were used if SAM pre-flight or testbed data were not available.

Eq. 1 $RMR_{X/Y} = I_{X, spectrum} / I_{Y, spectrum}$

Each RMR was then applied to the signal intensity for each time stamp of Y measured by SAM (Y_m) in counts per second (cps) to determine the amounts to be removed from one or more volatiles (volatiles A, B, etc.) from X measured by SAM (X_m) (Eq. 2a-c). Importantly, all mass channel data measured by SAM was first mildly smoothed (11-point moving average) to some reduced analytical noise. Mass channel corrections also required that the data of different m/z profiles be checked for matching time stamps so that data of the same scan were used in each calculation.

Eq. 2a $X_c = X_m - (Y_m * RMR_{X/Y})$

Eq. 2b $X_c = X_m - (Y_m * RMR_{X/Y \text{ for volatile A}}) - (Y_m * RMR_{X/Y \text{ for volatile B}})$

Eq. 2c $X_c = X_m - (Y_m * RMR_{X/Y \text{ for volatile A}}) - (Y_m * RMR_{X/Y \text{ for volatile B}})$
$- (Y_m * RMR_{X/Y \text{ for volatile C}})$

Corrections to the m/z 78 mass channel are given here as an example and the explanation for these corrections is given in the "Data Processing: EGA mass profile corrections for SAM instrument background and dichloromethane" section. In this case, the fully corrected m/z 78 profile (m/z 78c) used in interpretations reflects the presence of benzene and related single-ring aromatics that produce a m/z 78 ion (e.g., aryl ethers) in evolved gases, i.e., the "volatile of interest." To remove contributions from TFMA and TBDMS-Cl (when applicable) from the SAM instrument background, the RMR of m/z 78 to 127 was calculated from the TFMA mass spectrum, the RMR of m/z 78 to 77 was calculated from the TBDMS-F mass spectrum, and the RMR of m/z 78 to 93 was calculated from the TBDMS-Cl mass spectrum (Eq. 3a-c). Each data point in the m/z 78c profile ($X_{c,78}$) for each sample according to Eq. 4a, except for Confidence Hills which required an additional correction for TBDMS-Cl contributions to m/z 78 (Eq. 4b).

Eq. 3a $RMR_{78/127 \text{ for TFMA}} = I_{78} / I_{127}$ from the TFMA mass spectrum

Eq. 3b $RMR_{78/77 \text{ for TBDMS-F}} = I_{78} / I_{77}$ from the TBDMS-F mass spectrum

Eq. 3c $RMR_{78/93 \text{ for TBDMS-Cl}} = I_{78} / I_{93}$ from the TBDMS-Cl mass spectrum

Eq. 4a $X_{c,78} = X_{m,78} - (Y_{m,127} * RMR_{78/127 \text{ for TFMA}}) - (Y_{m,77} * RMR_{78/77 \text{ for TBDMS-F}})$

Eq. 4b $X_{c,78} = X_{m,78} - (Y_{m,127} * RMR_{78/127 \text{ for TFMA}}) - (Y_{m,77} * RMR_{78/77 \text{ for TBDMS-F}})$
$- (Y_{m,93} * RMR_{78/93 \text{ for TBDMS-Cl}})$

Data Processing: EGA mass profile corrections for SAM instrument background and dichloromethane

Mass profiles of interest for potential thiophene and aromatic compounds were corrected for contributions assumed to be from known SAM instrument background, though it is uncertain if some dichloromethane is from the sample (*40*). See "Characterization of SAM instrument background in EGA derived from derivatization reagents" section above for more detailed information of the source of the molecules. Applicability and utility of corrections were explored on a case-by-case basis. Details of that investigation are presented here.

TFMA (2,2,2-Trifluoro-N-methylacetamide) is clearly detected in EGA by the correlated *m/z* 58 and 127 profiles. TFMA mainly evolves below 350°C in CB2-5 and JK4, below 400°C in MJ, CH, and TP samples, and below 525°C in BK. In nominal blanks, TFMA evolves up to 800°C. SAM experimental modifications for the CB6, CB7, and CBblank2 tests were effective at eliminating this MTBSTFA reaction product all together. In other samples, TFMA may be contributing ion fragments of other masses of interest (Table S5) at higher temperatures due to its tailing evolution (e.g., Fig S7). No TFMA correction was applied to reported *m/z* 97 or 128 data because these masses are of sufficiently low RMR (<0.02) compared to *m/z* 58, the base peak. In contrast, TFMA contributions to *m/z* 78 (diagnostic for benzene) are significant enough to warrant correction. A comparative test was conducted to determine which m/z value to use as representative of TFMA contributions to the *m/z* 78 profile. Two options for the TFMA correction were considered: Assuming *m/z* 58 is solely from TFMA and using it for the correction, or using the much lower intensity, *m/z* 127 channel (RMR of 0.24) for the correction. The former approach results in over-correction since it ignores small amounts of *m/z* 58 contributed from ≥C4 aliphatic compounds. Correction based on *m/z* 127 may result in under-correction due to the weaker intensity representative for TFMA. There is no single solution. Thus *m/z* 127 was used to correct for TFMA contributions to the *m/z* 78 signal and further correction for the baseline was applied if necessary to remove residual signal suspected of a TFMA peak. This approach was taken to be certain of the presence of some sample-related signal that suggest a benzene composition. All data for *m/z* 78c is reported with TFMA contributions removed using *m/z* 127.

TBDMS-F (*tert*-butyldimethylsilyl fluoride) also contributes to *m/z* 78 as well as *m/z* 134. It is detected below 500°C in CB2-5, JK4, CH, MJ, TP, and BK samples. In CB6-7, TBDMS-F is barely detectable below 500°C. CB blank1, CB blank2, and CH blank show a release up to at least 700°C. TBDMS-F corrections were investigated assuming all of *m/z* 77 above 400°C is from TBDMS-F. As with the TFMA correction above, the TBDMS-F probably over-corrects the data since it ignores lesser contributions of *m/z* 77 from possible sample-derived aromatic compounds. Despite this methodology shortcoming, a TBDMS-F correction applied to *m/z* 134 and *m/z* 78c profiles had no qualitative impact on interpretations of peak presence and absence, but the

TBDMS-F correction applied to *m/z* 78c did influence the peak areas on a qualitative basis. Thus, all *m/z* 78cc data is reported with an additional TBDMS correction. No correction for TBDMS-F was applied to *m/z* 134.

TBDMS-Cl (*tert*-butyldimethylsilyl chloride) is a third potential contributor to *m/z* 78 but it is readily identifiable by the correlated *m/z* 93 and 95 traces. The only EGA profiles where its presence is suspected is in CH sample at ~500°C, so the TBDMS-Cl contribution of *m/z* 78 was subtracted from the mass channel in addition to the above.

Cyanogen bromide is observed below 500°C as strongly correlated *m/z* 105 and 107 profiles in a ~1:1 ratio in JK4, CB2-5. At higher temperatures and in other samples, qualitative correlations are observed, but the 105/107 mass ratio is inconsistent with CNBr, suggesting contributions from other components that contribute both *m/z* 105 and 107 in different proportions. No corrections for CNBr were applied to data.

Bromomethane (BM) is observed in JK4, CB6, CB7 CH, TP, and BK samples at <500°C, as strongly correlated *m/z* 94 and 96 profiles in a ~1:1 ratio and may contribute to *m/z* 91. However, the variations in the *m/z* 91 mass channel for samples above 500°C are large and the RMR for 91/94 is small enough (0.07) that BM corrections had no quantitative or qualitative impact on the profile at an interpretable level.

Chloromethylpropene was also investigated as a contributor to the *m/z* 91 profile. It is difficult to identify in EGA due to a lack of diagnostic ions. More importantly, the 90/91 mass ratio observed contradicts the expected ratio if most of *m/z* 91 was from chloromethylpropenes. Thus, no mass channel corrections were applied to *m/z* 91.

Dichloromethane can interfere with the detection of thiophene (TH) by EGA via its diagnostic mass, *m/z* 84. Only in CH and MJ samples does DCM evolution (confirmed by both *m/z* 84 and 86 for its ^{35}Cl and ^{37}Cl isotopologues) overlap with thiophene. There is no indication of DCM release above 400°C in other analyses, based on the lack of correlative variations in the *m/z* 84 and 86 profiles. In CH and MJ samples, the *m/z* 86 channel that records ^{37}Cl-DCM evolution is complicated by the evolution of SiF$_4$ above 766°C also observed only in these two samples. Therefore, before applying the DCM correction to *m/z* 84 for assessment of thiophene, the *m/z* 86 channel was first corrected for contributions from SiF$_4$ derived from an unknown mineral source in samples. This was achieved most effectively by baseline subtraction using *m/z* 85 (base peak of SiF$_4$) as a guide for the peak temperature range (see below for a description of baseline subtraction) to generate *m/z* 86c. The *m/z* 84 channel for CH and MJ samples was then corrected for contributions from dichloromethane (using *m/z* 86c).

SAM instrument background also contributed to signals interpreted as aliphatic hydrocarbons or cyanides (e.g., methylpropene, propene, ethylene, methane, and hydrogen cyanide), however these were corrected using background subtraction (see "Data Processing: Baseline subtraction of SAM instrument background above 400°C" section) guided by SAM blank and laboratory experimental results.

Data Processing: EGA mass profile corrections for other volatiles

The following mass channel corrections were applied to mass channels diagnostic of particular gases:

- ***m/z* 62c** is derived from the *m/z* 62 channel (diagnostic of dimethylsulfide) corrected for contributions from carbonyl sulfide (*m/z* 60)

- *m/z* **47c** is derived from the *m/z* 47 channel (diagnostic of methane thiol) corrected for contributions from dimethylsulfide (*m/z* 62c)
- *m/z* **45c** is derived from the *m/z* 45 channel (diagnostic of CO_2 isotopologue) corrected for contributions from dimethylsulfide (*m/z* 62)
- *m/z* **28c** is derived from the *m/z* 28 channel (assumed to be mostly from carbon monoxide with lesser amounts from possible hydrocarbons) corrected for contributions from CO_2 (*m/z* 45 for the CO_2 isotopologue; *m/z* 44 saturates the detector), carbonyl sulfide (*m/z* 60) and dimethylsulfide (*m/z* 62c)
- *m/z* **29c** is derived from *m/z* 29 channel corrected for contributions from isotopically enriched CO base on *m/z* 28c
- *m/z* **32c** reflects oxygen evolution and it was derived from *m/z* 32 channel corrected for significant contributions from SO_2 (*m/z* 66). RMR for 66/32 used in calculations was 6.3e-01 ± 1.0e+01 (1σ standard deviation) and was based on five analyses of calcite/melanterite on the SAM flight model before launch. The SO_2 isotopologue is used since *m/z* 64 saturates the detector on occasion.
- *m/z* **34c** reflects dihydrogen sulfide evolution and it was derived from the *m/z* 34 channel corrected for contributions from SO_2 (*m/z* 66) and O_2 (*m/z* 32c). RMR for 66/34 used in calculations was 4.8e-02 ± 2.3e-01 (1σ standard deviation) and was based on five analyses of calcite/melanterite on the SAM flight model before launch. RMR for 34/32 used in calculations, 4.0Ee-03 ± 2.0e-01 (1σ standard deviation), is the ratio observed in Rocknest analyses and assumes the low temperature evolution of *m/z* 34 reflects the main O_2 release (*3*).

Data Processing: Smoothing and implications on peak maxima and minima in EGA

Data was smoothed using an 11-point moving average followed by second 21-point moving average since this two-step smoothing was found to reduce most analytical noise without compromise to the identification of peak maxima and valley minima. Peaks and valleys in the smoothed EGA data are not smoothing artifacts as determined by comparison to data smoothed using only 5-, 11-, 21-, and 31- point moving averages. Consequently, temperatures assigned to peaks have an error of ± 25°C. Peak areas (described in the baseline subtraction section below) determined using the smoothing approach described here compared to peaks areas using raw data indicate that smoothing introduces 5% uncertainty (1σ standard deviation for many m/z profiles and many samples).

Data Processing: Baseline subtraction of SAM instrument background above 400°C

Figures show EGA profiles with the trending baseline subtracted (Fig. S11) from the profile. The baseline subtraction approach assumes that all organic volatiles that begin their evolution below 500°C are potentially derived from the instrument background (i.e., MTBSTFA reagent and its reaction products; see "Characterization of SAM instrument background in EGA from derivatization reagents" section above). While this may not be the case for all molecules (e.g., chlorobenzene (*1*)) it was a necessary simplification in the data processing rationale. It was also assumed that the background volatiles that started evolving below 500°C are best

characterized by a main peak and an extended tail into higher temperatures for each *m/z*. These two features are observed in SAM analyses of samples and blanks as well as laboratory EGA tests with the derivatization reagents (Fig. S7). For blanks, the main peaks tend to reach its maximum

Furthermore, it was assumed that all m/z profiles for mudstone analyses were impacted by combustion. All mudstones analyzed by SAM showed an O_2 release attributed to the decomposition of oxychlorine phases (e.g., perchlorates, chlorates, etc.) that largely occurred below 500°C and this O_2 results in combustion of organic components (*1*, *2*, *3*, *39*, *40*, *44*). In EGA, combustion is indicated by the release of CO_2 closely associated the O_2 release. A consequence of combustion, particularly for readily ignitable volatile components, is an interruption in their detectable signal because there is a momentary loss in actual volatiles. Examples of this interruption in signal are shown in the CF_3 (orange line) and methylpropene (pink line) at ~280°C for the Laboratory: TBDMS-FS120 + 1wt.% Fe(II)-Perchlorate EGA profiles of Figure S7. In some cases, this feature was easily recognizable because the m/z profiles of interest showed a valley during O_2 release followed by a peak that fit the tailing trend of the main peak. In other cases, it was not so obvious. In those cases, it was assumed that the first peak observed in the *m/z* profile on interest that followed the O_2 release, was the last portion of the main peak. Such is the case for the Mojave EGA *m/z* 43 profile in Figure S11. Although we cannot be certain that combustion is impacting every *m/z* profile in the manner described, a conservative approached claiming this assumption was adopted to rule out as many known and suspect contributions from the SAM instrument background.

The assumptions were used to set two criteria for the baseline: 1) the baseline curve must approximate the tail of main peak that occurred below 500°C, and 2) the baseline curve must begin immediately after any post-combustion peak that may represent a return to release of components associated with the main peak. Each baseline was drawn using OriginPro software (Origin Lab Corporation, USA) and the "spline" baseline option on smoothed data. Baselines were determined by the person conducting the data processing to meet the two criteria. Baseline subtraction from each *m/z* profiles results in a flat line prior to the start of the baseline and the flat line denotes signal that is not relevant to the subsequent analysis. Accordingly, blanks with main peaks extending well past the 500°C mark have processed EGA profiles with a flat line past 500°C. If there was no main peak in a *m/z* profile, then the baseline was drawn as a horizontal line from the lowest point in the profile after 500°C.

EGA profiles shown in figures and abundance estimates found in tables reflect results using the most cautious estimate of SAM background contributions to the *m/z* profile. As such, estimated abundances reflect the lower limit of non-background, organic components released at high temperature. Further, these estimates take no account of any organic components remaining in the sample residue after heating. Estimated abundances have propagated errors that include a 30% uncertainty in peak integration (1σ standard deviation) that was determined by drawing different baselines for several *m/z* profiles and for different SAM analyses. This uncertainty was generalized and applied to all abundance calculations.

Quantitation: Thiophenes, aromatics and C1-C2 sulfur compounds observed in EGA

The goal of the molar estimate was to establish a lower limit for the order of magnitude of carbon abundance. Thus, a conservative approach was taken to assess molecular abundances for gases evolved at high temperature that employs baseline-subtracted mass channels as described

above such that the resulting abundances represent a lower limit to the amount present. Molar abundances were estimated assuming the molecule diagnostic of a mass channel was solely responsible for the signal observed unless the mass profile was previously corrected (described above). For the C1-C2 sulfur compounds (COS, CS_2, CH_3SH, and $(CH_3)_2S$) the baseline was assumed horizontal from the time marker "start of pyrolysis," unless there appeared to be an overall decreasing background trend (e.g., most blanks) and then a slope was used. If a slope was applied it was based on slope established by the earliest portion of the pyrolysis.

It was assumed that the primary ion used for identification of molecules in EGA solely reflected contributions from the designated molecule. Estimates of molar abundances require application of 70-eV electron-impact ionization cross section (ICS) constants as either total ionization cross section of a molecule ($TICS_M$) or partial ionization cross sections for an ion fragment of the molecule ($PICS_{ion}$) (Table S7). When TIC_MS and $PICS_{ion}s$ had not been published, either they were calculated using the Binary-Encounter-Bethe (BEB) model by Karl Irikura (Chemical and Biochemical Reference Data Division, National Institute of Standards and Technology, Gaithersburg, MD), or the relative molar response (in this case, RMR is the ratio of one ion to the sum of ions for the molecule (M) and is also called the molecular-ion branching fractions) was applied to the $TICS_M$ according to Equation 5 in order to derive a PICS(ion). RMRs were based on NIST mass spectral references and were assumed to have 20% uncertainty (*33*). $TICS_{MS}$ calculated from the BEB model were also assumed to have 20% uncertainty (*48*) if uncertainty was not specified in publication. Of note, the SAM QMS was tuned to match the relative intensities in the NIST mass spectrum of PFTBA and thus we expect observed molecular spectra to closely match NIST spectra.

Cross sections were applied to estimate molar abundances according to Equation 6. The CO_2 calibration factors were determined using pre-flight data of calcite (*49*). Specifically, those calibration factors are: 2.012808 x 10^{-6} ± 7.371886 x 10^{-8} nanomol calcite/counts CO_2 for SAM FM oven 1, 1.681215 x 10^{-6} ± 1.399504 x 10^{-7} nanomol calcite/counts CO_2 for SAM FM oven 2. A single portion was assumed for all blanks except the repeated analysis of the CB6 material (CB6r). Single portion size of drilled fines was 45 ± 18 mg (135 ± 31 mg for triple portions). Results are presented as nanomole C or S in Table 1, S1 and S4. Results calculates as nanomole molecules are in Table S8. Respective concentrations are given in Table S9 and S10.

Eq. 5. $PICS_{ion} = TICS_M * RMR_{ion/M}$

Eq. 6. nanomole of molecule = CO_2 calibration factor * [Peak Area of ion / $PICS_{ion}$],
where CO_2 calibration factor = nanomol calcite/counts CO_2 * $TICS_{CO2}$

Quantitation of aromatic contributions from the m/z 105 profiles, which may reflect various alkylbenzene contributions or benzoate ion, such as from benzoic acid, were limited to the availability of ionization cross sections. Only benzoic acid ICSs were available. Thus, for quantitation purposes, benzoic acid was used as a proxy for carbon and molecular abundances reflected in the m/z 105 profiles.

Quantitation: Aliphatic compounds observed in EGA

Aliphatic compounds abundance estimates are, at best, semi-quantitative and the calculations require several assumptions. Mass profile data of EGA reflects parent and fragment ions of the bulk gas evolving from the oven at any time during the experiment. The possible molecular contributions are numerous and the uncertainty is difficult to constrain.

In general, hydrocarbon pyrolysis products tend to have higher abundances in low carbon number structures compared to many carbon structures. This applies to molecular groups, such as alkanes and alkenes. Alkane abundance tends to be greater than or equivalent to alkene abundance (*13*). These generalities are assumed for mudstone aliphatic compound abundance estimates. In EGA, disparate fragmentation patterns for C1-C5 components complicate such relationships, especially if the C1-C5 contributions are derived from >C5 parent molecules that have significantly weaker ion intensities for fragments that exceed 5 carbons. Such is typical of aliphatic components. The C1-C5 hydrocarbon contributions observed in Gale crater mudstones may be from a diverse suite of molecules that extend to higher carbon identities, but for the sake of simplifying the abundance estimates, only C1-C4 molecular components are considered and in proportions that reflect C1 > C2 > C3 > C4 and alkane ≥ alkene trends. Further, the peak areas for *m/z* 15 and *m/z* 56 were assumed to reflect contributions primarily from methane and butenes, since the ions have strong relative intensities in these spectra and are the only reasonable sources with the C1-C5 constraint. Estimates maximize the saturated and unsaturated hydrocarbon inputs and account for most of the residual *m/z* 30, 27, and 26 signals with the addition of NO and HCN.

Estimates are modeled using step-by-step subtraction of the signal intensities attributable to each component. Each step resulted in a set of residual ion peak areas. Residual ion values were maintained within the propagated errors for initial integrated *m/z* profile peak areas. For example, a percentage of the *m/z* 15 counts that make up the total *m/z* 15 signal was assigned to methane (usually 90-99%). Since methane has few ions in its mass spectra, no subtractions from total counts for other *m/z* values were made. Next, a percentage of *m/z* 30 counts was assumed to be from ethane. Correlative amounts of other ions based on the ethane mass spectra were subtracted from residual *m/z* counts. This process continued with propane (*m/z* 29), ethene (*m/z* 27), propene (*m/z* 41), 1-butene and 2-butene (*m/z* 56), and HCN (assigned to leftover *m/z* 27). Not all of the residuals were expended and the percentage of the sum of peak areas represented is reported. Modeled *m/z* counts attributed to each molecule were then used to calculate nanomole carbon abundances of each aliphatic compounds. Percentages used for each step were adjusted until the alkane-alkene pattern described above was achieved. Total aliphatic compounds abundances and propagated errors are given in Table 1. Respective concentrations are given in Table S10.

Quantitation: GCMS data

Estimated abundances of molecules detected in GC (Table S1) were determined by comparison to the five measurements of hexane conducted on the SAM instrument during preflight calibration (*10*). Hexane calibration error is propagated from the standard error of the hexane measurements (14.2% of average) and hexane TICS error (Table S7).

A Gaussian fit was applied to detected peaks. For each molecule quantified in GC data, the total ion signal for the molecule was calculated from the sum of integrated peak areas and extrapolated peak areas for the other masses based on the RMR from NIST mass spectra (*33*). The

sum of peak areas was assumed to be equivalent to the total ion count for the molecule. Total ionization cross sections for both hexane (TICS$_{hexane}$) and the selected molecule (TICS$_M$) detected in GC were applied in the molecular abundance calculation (Eq. 7). GCMS quantitation errors are propagated from hexane calibration error, peak integration error (assumed 14.2%), and TICS$_M$ errors (Table S7).

Eq. 7   nanomole of molecule = Hexane calibration factor * Sum of Peak Areas / TICS$_M$,
where hexane calibration factor = nanomole hexane/counts hexane * TICS$_{hexane}$

Analog Tests: SAM Testbed EGA method for Murchison meteorite

A powdered aliquot of the Murchison meteorite (USNM 6650) was acquired from the Smithsonian Institution. Six milligrams were added to a small nickel cup with ashed quartz wool to hold it in place. The capsule was lowered into a quartz cup in the SAM testbed SMS using a pronged grabbing tool. It was later run using similar analytical conditions as CB3 with the testbed in the Mars environmental chamber set to conditions similar to those experienced by SAM during martian analyses. EGA results are presented in Fig. S9.

Analog Tests: Laboratory EGA analysis of the Tissint meteorite

A small chunk of the Tissint martian meteorite (87 mg) was very finely powdered in an agate mortar with pestle that was first rinsed once with acidic methanol (2% HCl, 8% H$_2$O, 90% methanol) then three times each with methanol, acetone, and *n*-hexane before each use. All solvents were Fisher Optima brand. Hydrochloric acid used for making acidic methanol was double-distilled HCl from GFS Chemicals.

The Tissint martian meteorite was analyzed using a Frontier Autoshot-PY3030D pyrolyzer attached to an Agilent 7890A gas chromatograph (GC) fitted with a Restek MTX-5 (length 30 m, internal diameter 0.25 mm, and film thickness 0.25 μm), and 5975C inert XL mass spectrometer detector (MSD). The pyrolyzer was initially held at 50° C for 25 min and ramped at 35° C/min to 1050° C, where it was held for 5 min. Pyrolysis occurred under 25 mbar He and 12 ml/min flow. Volatiles were split at a ratio of 10:1 and carried by 1.5 ml/min helium flow through the inlet, column, and transfer line, all held at an isotherm of 300° C, to the MSD. The MSD was operated in select ion monitoring (SIM) mode and monitored 60 different *m/z* values with 50-ms dwell times. Masses were selected based on team recommendation and prior GCMS analysis of the 600-1000° C evolved gas fraction. EGA results are presented in Fig. S10.

Supplementary Text

Evaluation of SAM instrument background as a possible source of the organic detections

The SAM EGA instrument background, including derivatization-reagent (MTBSTFA) vapor deposition on samples (*40*), is not the source of the observed molecular diversity observed at high temperatures. First, SAM analyses and lab tests demonstrate that the majority of MTBSTFA derived products (Table S5) are volatile and thermally desorbed at <500ºC (Fig. S7),

especially in the presence of reactive and catalytic minerals, such as (per)chlorates, phyllosilicates, and iron oxides, common of all the mudstone samples analyzed by SAM. Although SAM blanks and laboratory tests with silica demonstrate that *tert*-butyldimethylsilyl- (TBDMS-) derivatized active OH sites on silica surfaces undergo pyrolysis above 500ºC, there is no indication of a correlative process occurring on samples having reactive and catalytic minerals (Fig. S7). In an effort to be extra cautious, all possible traces of suspect instrument background were removed in data processing. Second, MTBSTFA products in sample analyses are highly susceptible to oxidation by O_2 and chlorination because of oxychlorine decomposition below 550ºC. Third, there are no structures in the SAM EGA instrument background that contain >C4 carbon backbones. Methylthiophenes, C5-alkyl fragments, and aromatics are C5 or greater structures. Condensation reactions in the SAM oven below 500ºC would have produced volatile products and such reactions above 500ºC are unlikely. The only known non-SAM terrestrial contaminant is polytetrafluoroethylene (PTFE) shed from the diaphragm seal of the MSL drill bit assembly (*45*). Traces of perfluoroethene (<0.4 nmol C) observed in samples (Fig. S8) cannot explain the 60-90 nmol C of other organics evolved at high temperature in Mojave and Confidence Hills (Table 1) evolved at the same and higher temperatures. Theoretically, PTFE is a very unlikely precursor for the observed molecules in Mojave. Lastly, SAM observations are inconsistent with the delivery of other polymer or plasticizer contaminants (*50*).

Potential for chlorination of aromatic moieties in the SAM oven

Chlorobenzene, chloromethanes, and other chlorinated hydrocarbons were observed in EGA below 400ºC in the Cumberland drill sample from the Sheepbed mudstones at the base of Gale Crater (*1*) and interpreted to be reaction products of chlorine and organic carbon derived from martian sources. Analysis of the Mojave mudstone revealed chloromethanes release at 500-670ºC (Fig. 2A) that is accompanied by a peak in the *m/z* 112 profile at ~550ºC, which is consistent with a chlorobenzene release. The ^{37}Cl-chlorobenzene isotopologue in the *m/z* 114 profile (not shown) was not possible due to low signal-to-noise ratio to provide confirmation of this molecular assignment. These peaks coincide with a rise in HCl from an undetermined chemical component of the sample (*3*). This package of observations supports the possibility that aromatic moieties are being chlorinated in the SAM oven, a reaction supported by analog studies in the laboratory (*1, 47*), but it does not rule out the possibility that some chlorobenzene is directly evolving from the sediments. A second peak at ~780ºC in the *m/z* 112 profile is consistent with another chlorobenzene release in Mojave (Fig. 2B). Most likely, this is part of a release that began at ~550ºC and was interrupted by the oxygen release and lost to combustion.

Fig. S1. EGA profiles for thiophenes (A-D), thiols and sulfides (E-L), other volatiles (M-P), and O_2 and CO_2 (Q-T) with peaks indicating possible combustion in Murray mudstone samples: Confidence Hills blank (CH blank), Confidence Hills (CH sample), Telegraph Peak (TP) and Buckskin (BK). Legend shows volatile, *m/z,* and scaling factor for each profile. Symbols mark correlations between panes in peak maxima within ± 25ºC error due to signal smoothing. Axes and scaling factors are the same in Fig. 1-2 and S1-S6. Temperature placement of symbols are the same in Fig. 1-2, S1-S3. X-axis is scaled linearly to runtime to show the changing oven ramp rate and peak areas that scale to abundances. Y-axis scale bar in counts per second (cps) is for all panes. Profiles within panes are multiplied by scaling factors. All profiles are background subtracted, but profiles in A-D are shifted along the y-axis to show peaks clearly. "*i*", isotopologues in formulas. "c", corrections to profiles to remove other volatile contributions (*11*).
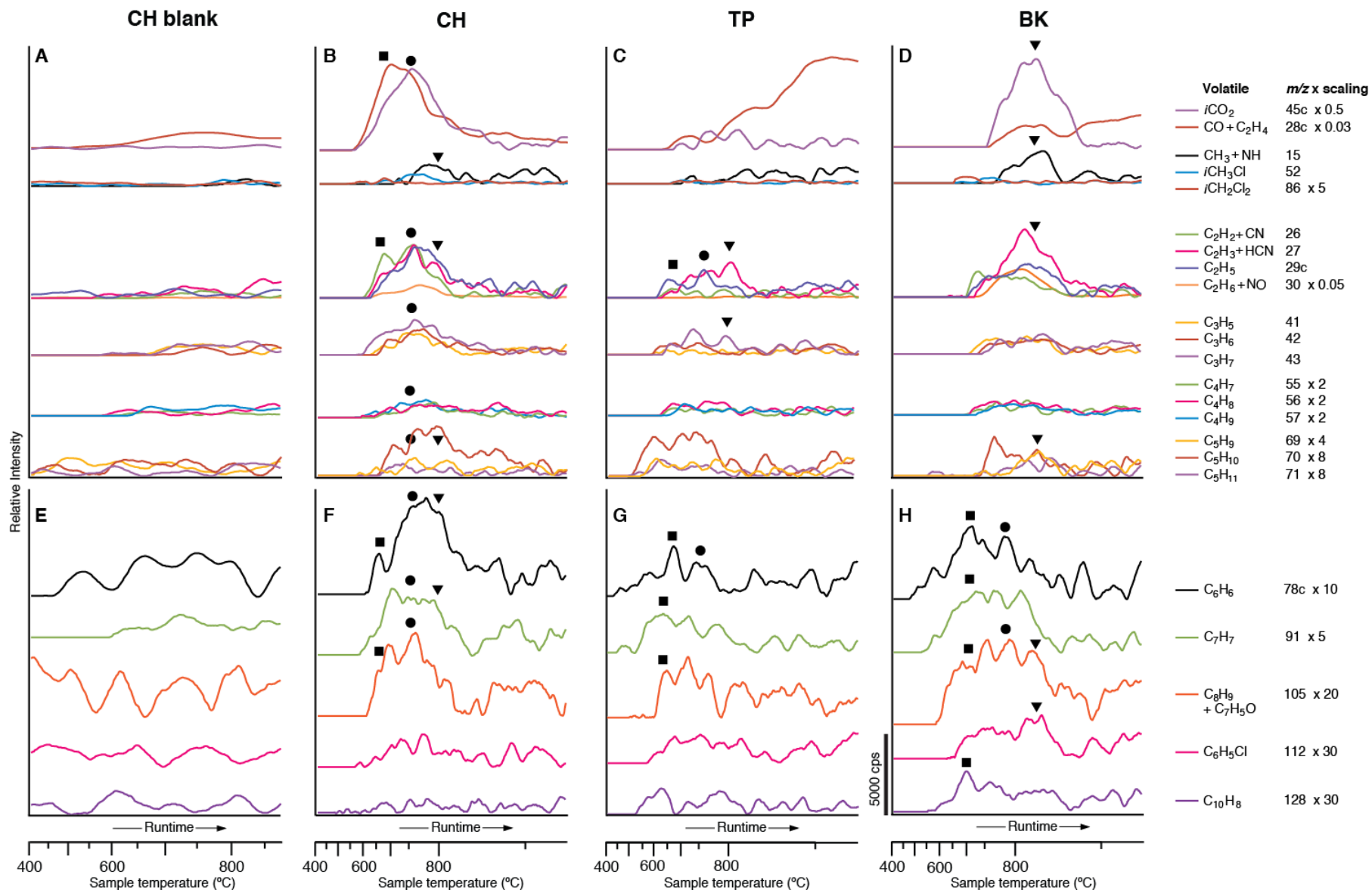
Fig. S2. EGA profiles for aliphatic (A-D) and aromatic (E-H) compounds in Murray mudstone samples: Confidence Hills blank (CH blank), Confidence Hills (CH sample), Telegraph Peak (TP) and Buckskin (BK). CO and CO_2 profiles are included in A-D. Legend and plotting details are described in Figure S1. All profiles are background subtracted and on the same scale after applying scaling factor. Profiles in A-D are grouped by carbon number and shifted along the y-axis to show peaks clearly. Profiles in E-H are similarly shifted.
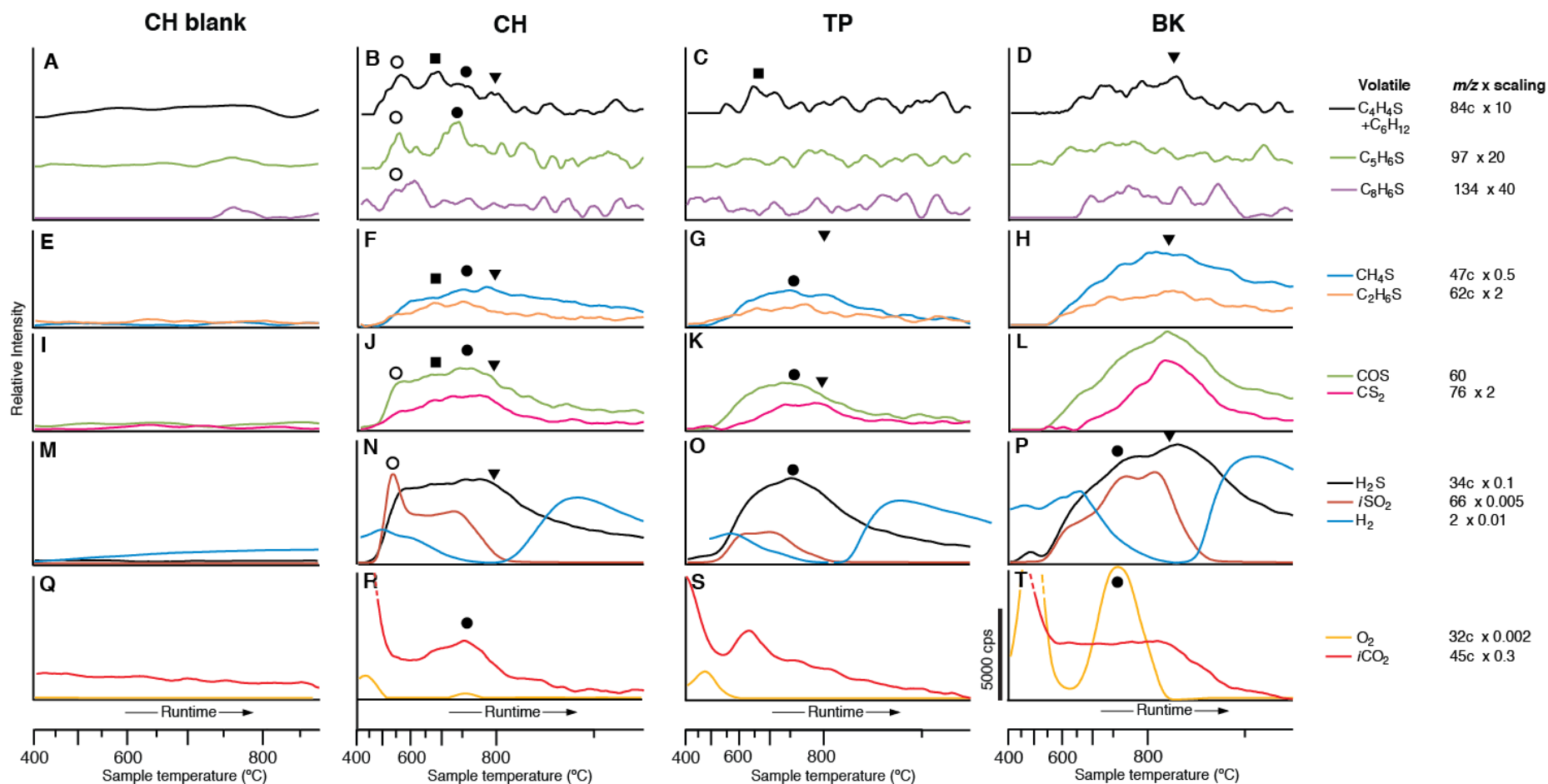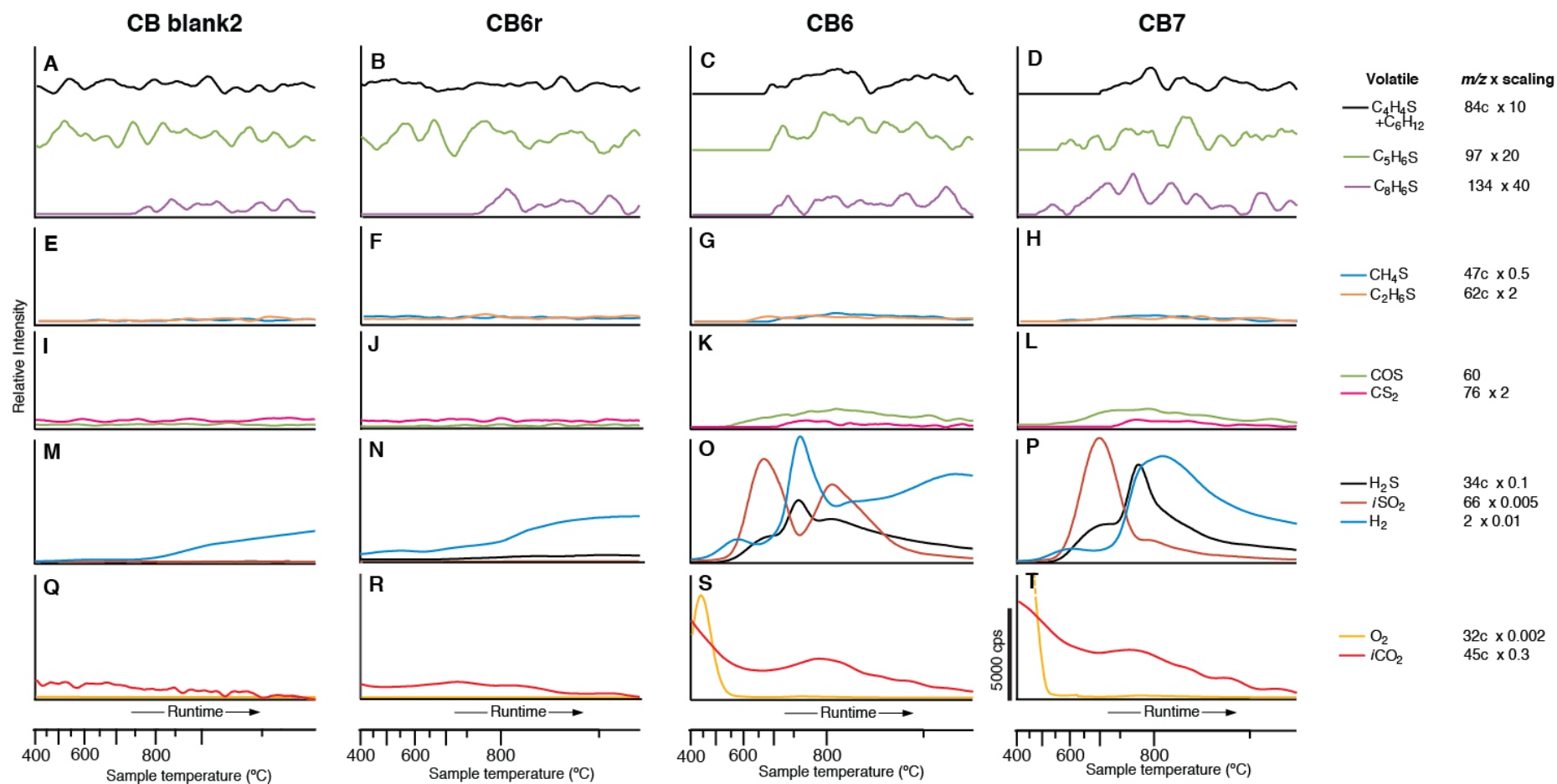
Fig. S3. EGA profiles for thiophenes (A-B), thiols and sulfides (C-F), other volatiles (G-H), and O_2 and CO_2 (I-J) with peaks indicating possible combustion in Sheepbed mudstone samples: Cumberland blank-1 (CB blank1) and John Klein-4 (JK4). Legend and plotting details are described in Figure S1. All profiles are background subtracted and on the same scale after applying scaling factor. All profiles are background subtracted, but profiles in A-B are shifted along the y-axis to show peaks clearly.
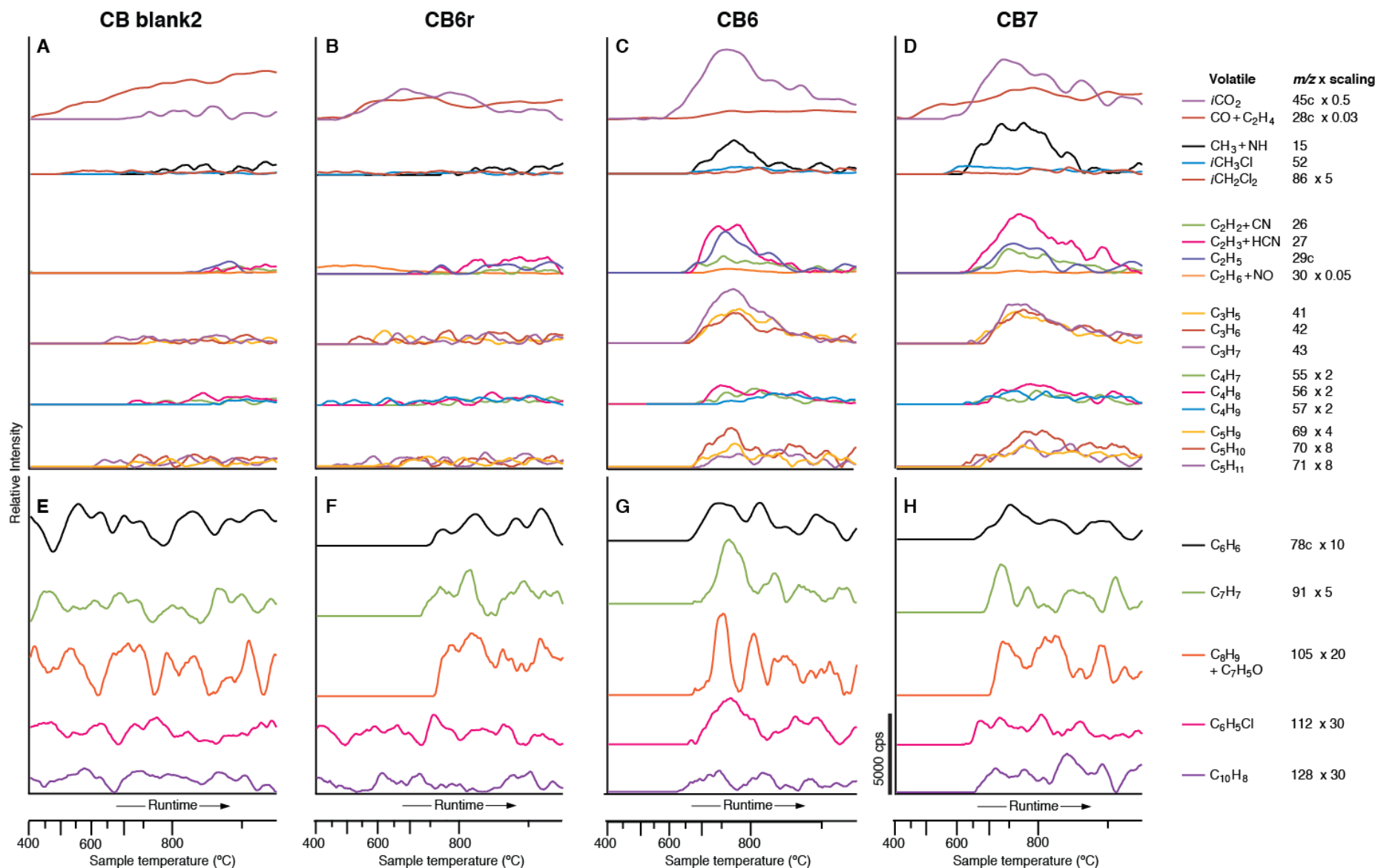
Fig. S4. EGA profiles for aliphatic (A-B) and aromatic (C-D) compounds in Sheepbed mudstone samples: Cumberland blank-1 (CB blank1) and John Klein-4 (JK4). CO and CO₂ profiles are included in A-B. Legend and plotting details are described in Figure S1. All profiles are background subtracted and on the same scale after applying scaling factor. Profiles in A-B are grouped by carbon number and shifted along the y-axis to show peaks clearly. Profiles in C-D are similarly shifted.
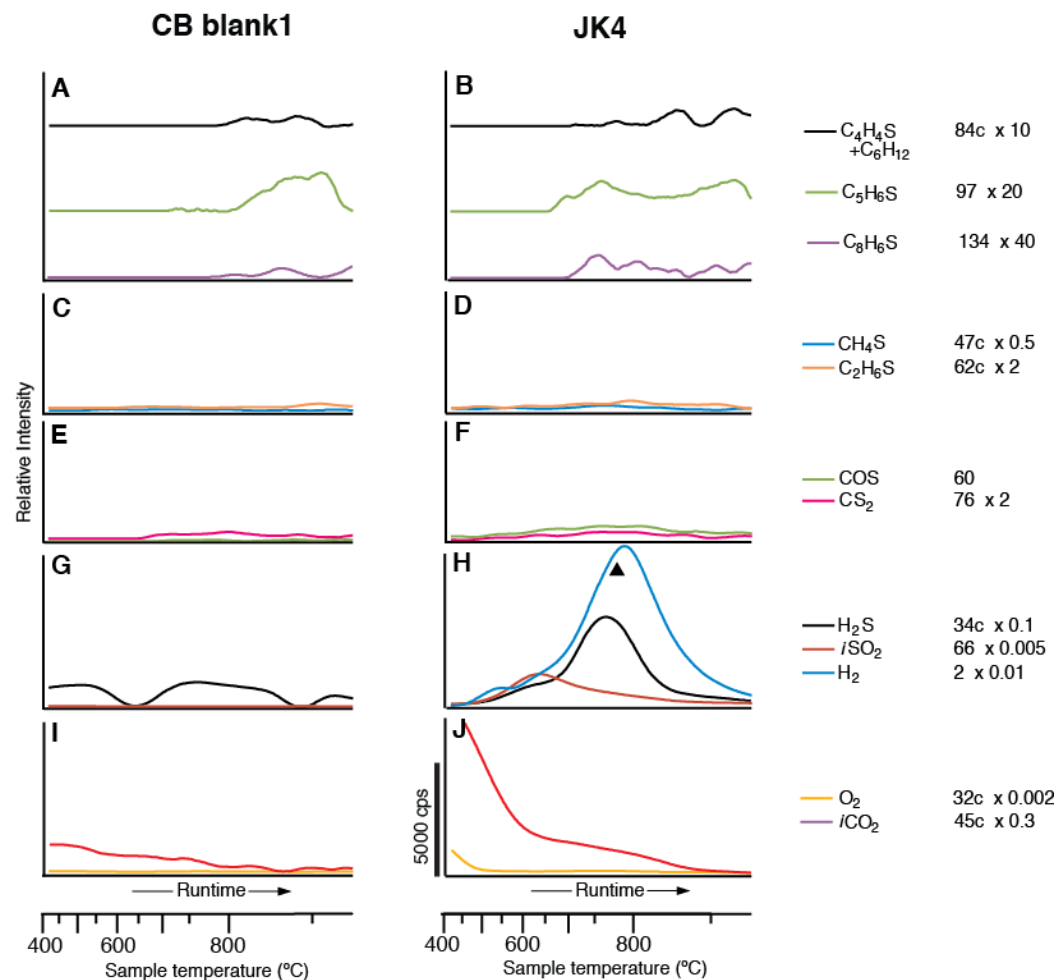
Fig. S5. EGA profiles for thiophenes (A-D), thiols and sulfides (E-L), other volatiles (M-P), and O_2 and CO_2 (Q-T) with peaks indicating possible combustion in Sheepbed mudstone samples: Cumberland blank-2 (CB blank2), Cumberland 6 reheat (CB6r), Cumberland 6 (CB6), and Cumberland 7 (CB7). Legend and plotting details are described in Figure S1. All profiles are background subtracted and on the same scale after applying scaling factor. All profiles are background subtracted, but profiles in A-D are shifted along the y-axis to show peaks clearly.

CB blank1   **JK4**

Volatile	m/z x scaling
iCO$_2$	45c x 0.5
CO+C$_2$H$_4$	28c x 0.03
CH$_3$+NH	15
iCH$_3$Cl	52
iCH$_2$Cl$_2$	86 x 5
C$_2$H$_2$+CN	26
C$_2$H$_3$+HCN	27
C$_2$H$_5$	29c
C$_2$H$_6$+NO	30 x 0.05
C$_3$H$_5$	41
C$_3$H$_6$	42
C$_3$H$_7$	43
C$_4$H$_7$	55 x 2
C$_4$H$_8$	56 x 2
C$_4$H$_9$	57 x 2
C$_5$H$_9$	69 x 4
C$_5$H$_{10}$	70 x 8
C$_5$H$_{11}$	71 x 8
C$_6$H$_6$	78c x 10
C$_7$H$_7$	91 x 5
C$_8$H$_9$ + C$_7$H$_5$O	105 x 20
C$_6$H$_5$Cl	112 x 30
C$_{10}$H$_8$	128 x 30
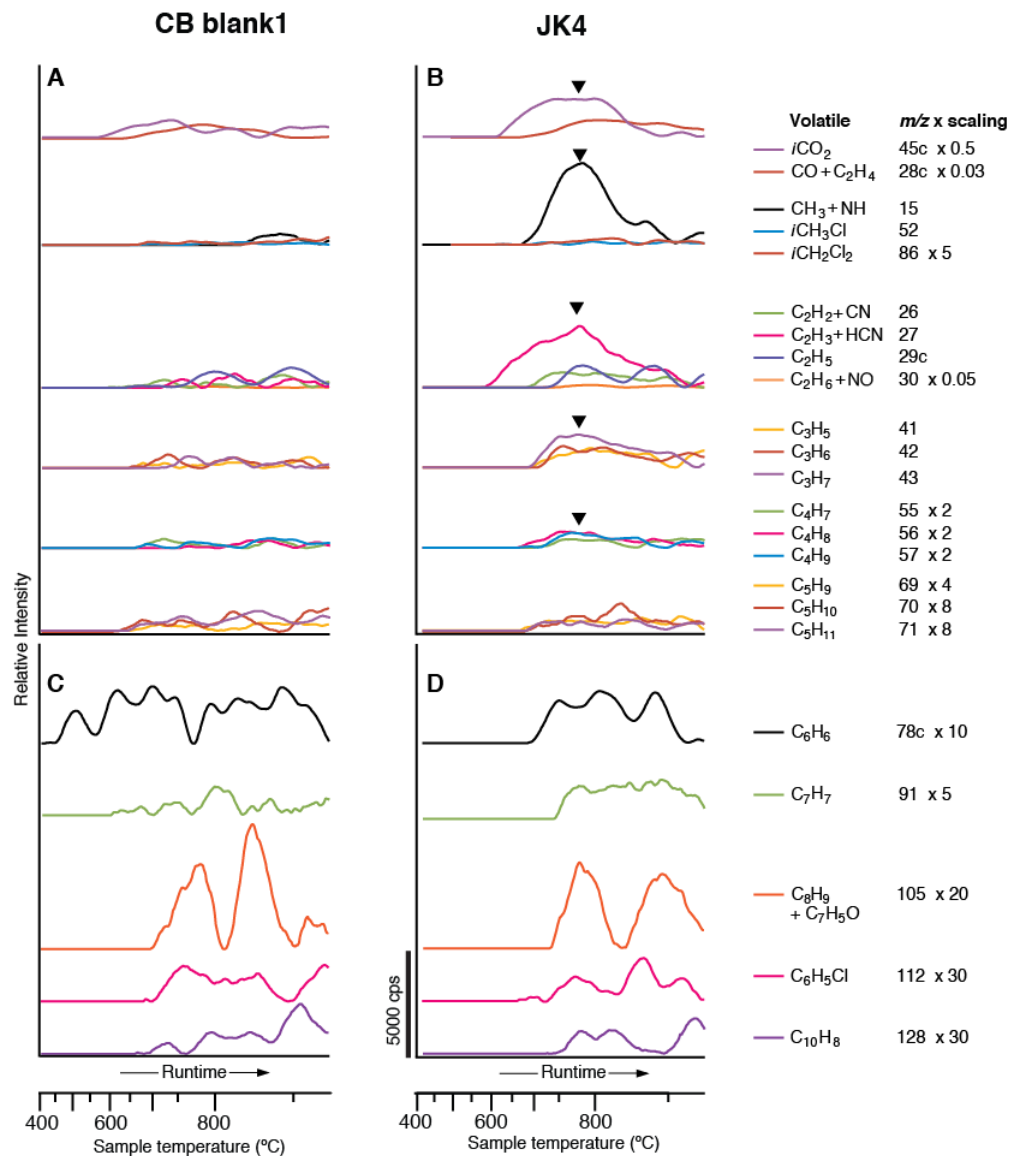
Fig. S6. EGA profiles for aliphatic (A-D) and aromatic (E-H) compounds in Sheepbed mudstone samples: Cumberland blank-2 (CB blank2), Cumberland 6 reheat (CB6r), Cumberland 6 (CB6), and Cumberland 7 (CB7). CO and CO$_2$ profiles are included in A-D. Legend and plotting details are described in Figure S1. All profiles are background subtracted and on the same scale after applying scaling factor. Profiles in A-D are grouped by carbon number and shifted along the y-axis to show peaks clearly. Profiles in E-H are similarly shifted.
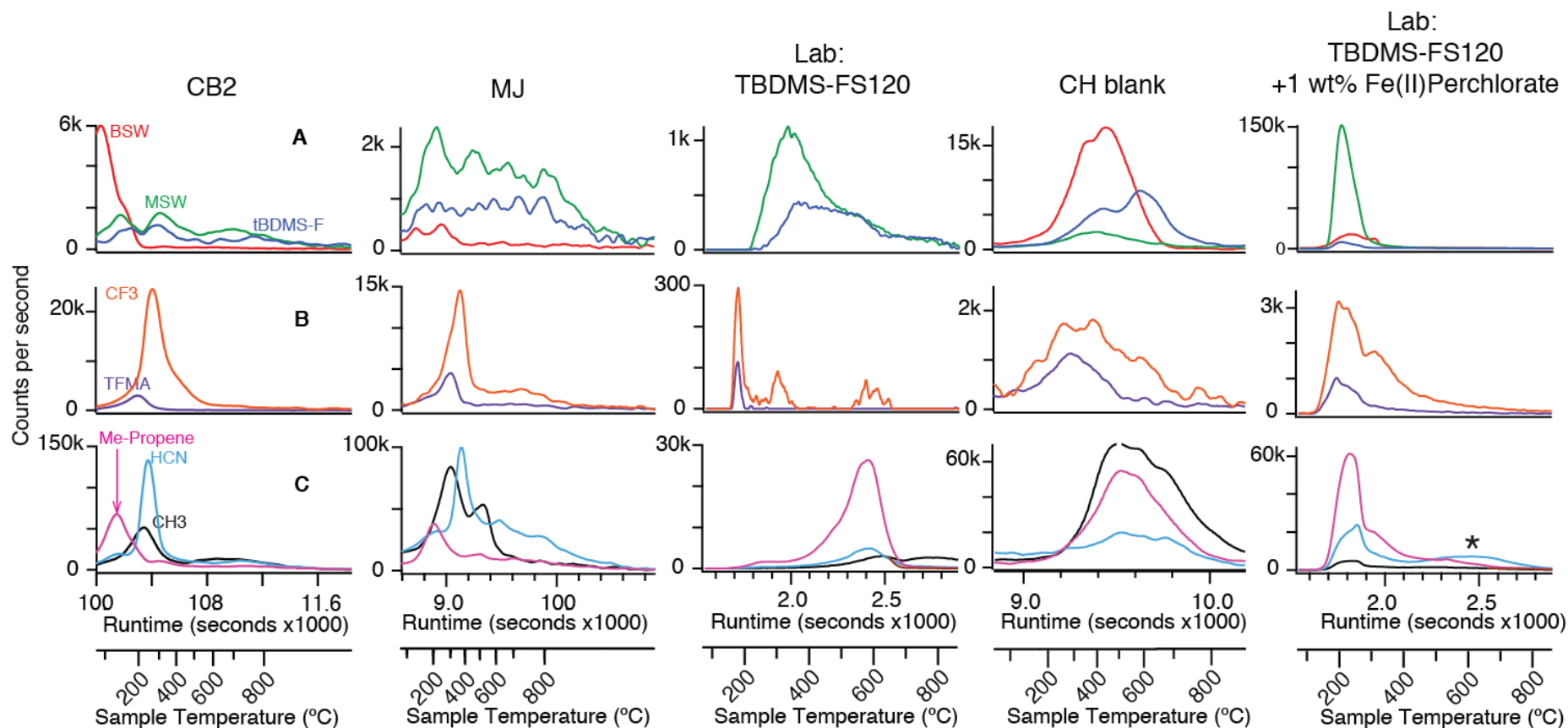
Fig. S7. Variations in the evolution of MTBSTFA reaction products in the SAM instrument background (Sheepbed mudstone: CB2, Murray mudstone: MJ, and CH blank) and in lab control experiments. TBDMS-organic derivatives thermally desorbed at low temperatures as shown in row A of plots show bisilylated water (BSW; m/z 147), monosilylated water (MSW or $tert$-butyldimethylsilanol; m/z 75), and TBDMS-F ($tert$-butyldimethylsilyl fluoride; m/z 77). Row B shows trifluoromethylacetamide (TFMA) related byproducts of silylation thermally desorb next as shown in B: TFMA (m/z 127) and CF3 fragment of other trifluorinated products (m/z 69). Row C shows pyrolysis products of remaining TBDMS-derivatives, especially derivatized OH sites on mineral surfaces are shown in C: methylpropene (m/z 41, 56, and 27), methane (represented by methylene: m/z 15). The asterisk indicates signals from trace contaminants in the perchlorate standard. Mass profiles are from laboratory EGA analysis of ashed fused silica (FS120; (51)) mixed with 1 wt% Fe(II) perchlorate and silylated with MTBSTFA at 25°C, 1 bar for 1 hour. Excess MTBSTFA was removed by gently flowing N₂(g) over the sample. Analytical conditions approximate those of SAM. The pattern observed above is representative of analyses with other perchlorates except for differences in the O₂ evolution temperature. X-axis is scaled linearly to runtime to show the changing oven ramp rate and peak areas that scale to abundances.

23
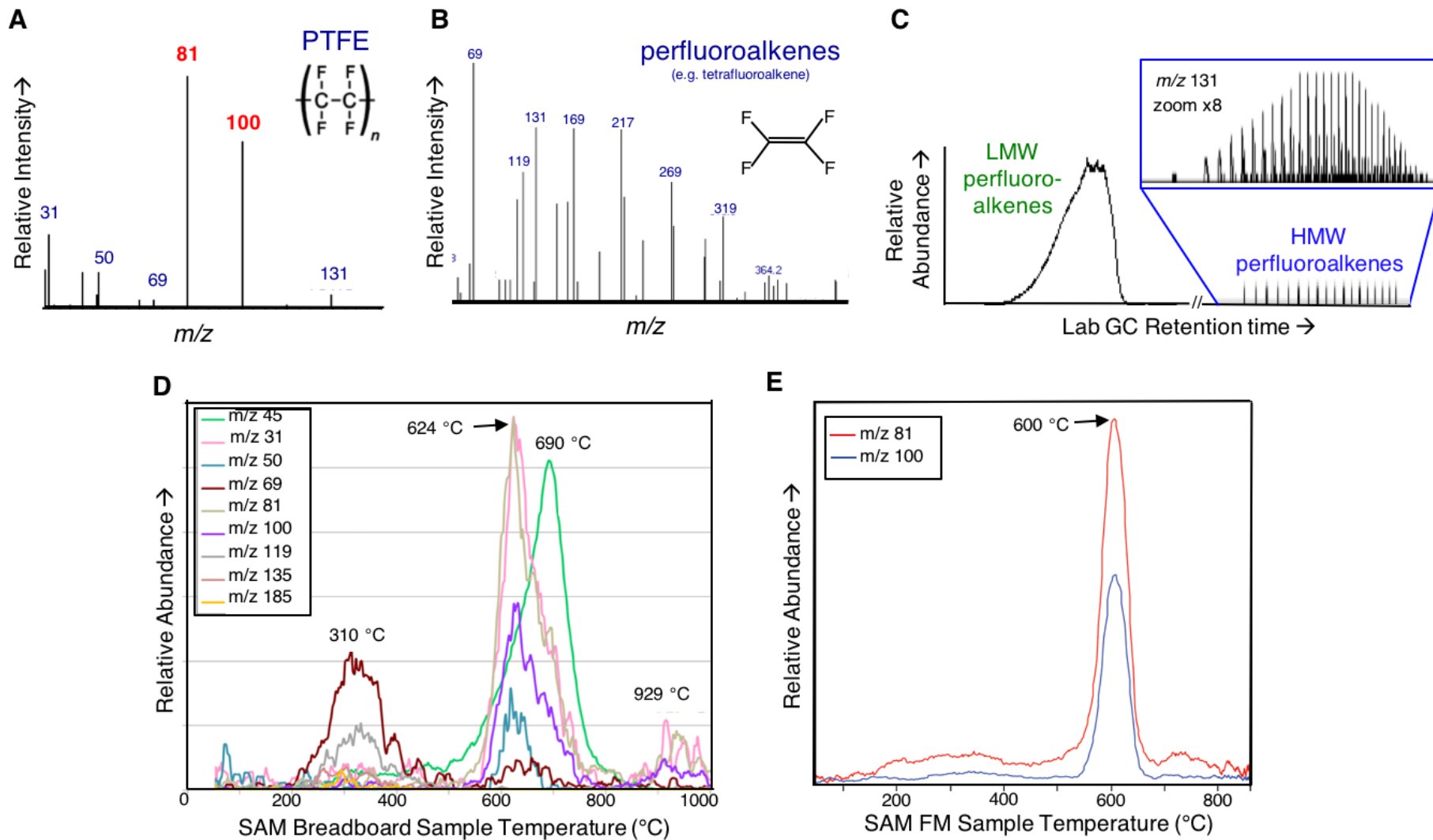
Fig. S8. Caption on next page.

Fig. S8. Polytetrafluoroethylene (PTFE; trademarked as Teflon by Dupont Co.) particles shed from the diaphragm seal in the MSL drill bit assembly were investigated for their impact on SAM EGA and GCMS. A) Mass spectrum of pyrolysate products. (Test sample: OCM SN48; scan # 4261). (A) Mass spectrum of low molecular weight (LMW) perfluoroalkene mixture (*52*) dominated by tetrafluoroethylene giving the strong *m/z* 81 and 100 signals (red). (B) Example mass spectrum for the high molecular weight (HMW) perfluoroalkene series. Key ion series for detection are $M^+ + 100n$, where M^+ = 69, 119, 131, and 181. (C) Laboratory pyrolysis-GCMS results for the diaphragm seal. Total ion chromatogram shows both LMW perfluoroalkenes (eluting from the GC column held at 35°C) and HMW perfluoroalkenes (elute from the GC column 250-300°C). Inset is the *m/z* 131 ion chromatogram that shows the >6 homologous series that make up the HMW perfluoroalkene component. (D) SAM breadboard EGA results for 55 mg of Saddleback basalt rock drilled at JPL using the testbed DBA and sieved to <150 micrometer particle size (Test sample: T28.1 G; analyzed May 2012). LMW and HMW perfluoroalkenes evolve at 560-800°C (max. at 624°C) and above 800°C (max at 924°C), respectively. Other unresolved hydrocarbon components at 200-500°C are from handling of the rock sample. Y-axis for *m/z* 45 (CO_2) is scaled to 5% to fit the axis of other ions. (E) SAM flight model (FM) EGA analysis of Telegraph Peak, which showed the greatest abundance of TFE (0.64 ± 0.32 nanomole; equivalent to 1420 ± 284 ppb TFE by mass and ~28.4 ppb C) due to drilling complications. TFE abundance in Mojave is 0.08 ± 0.04 nanomole (~184 ppb) or ~3.6 ppb C. TFE in Confidence Hills is 0.17 ± 0.09 nanomole (~378 ppb) or ~7.6 ppb C.
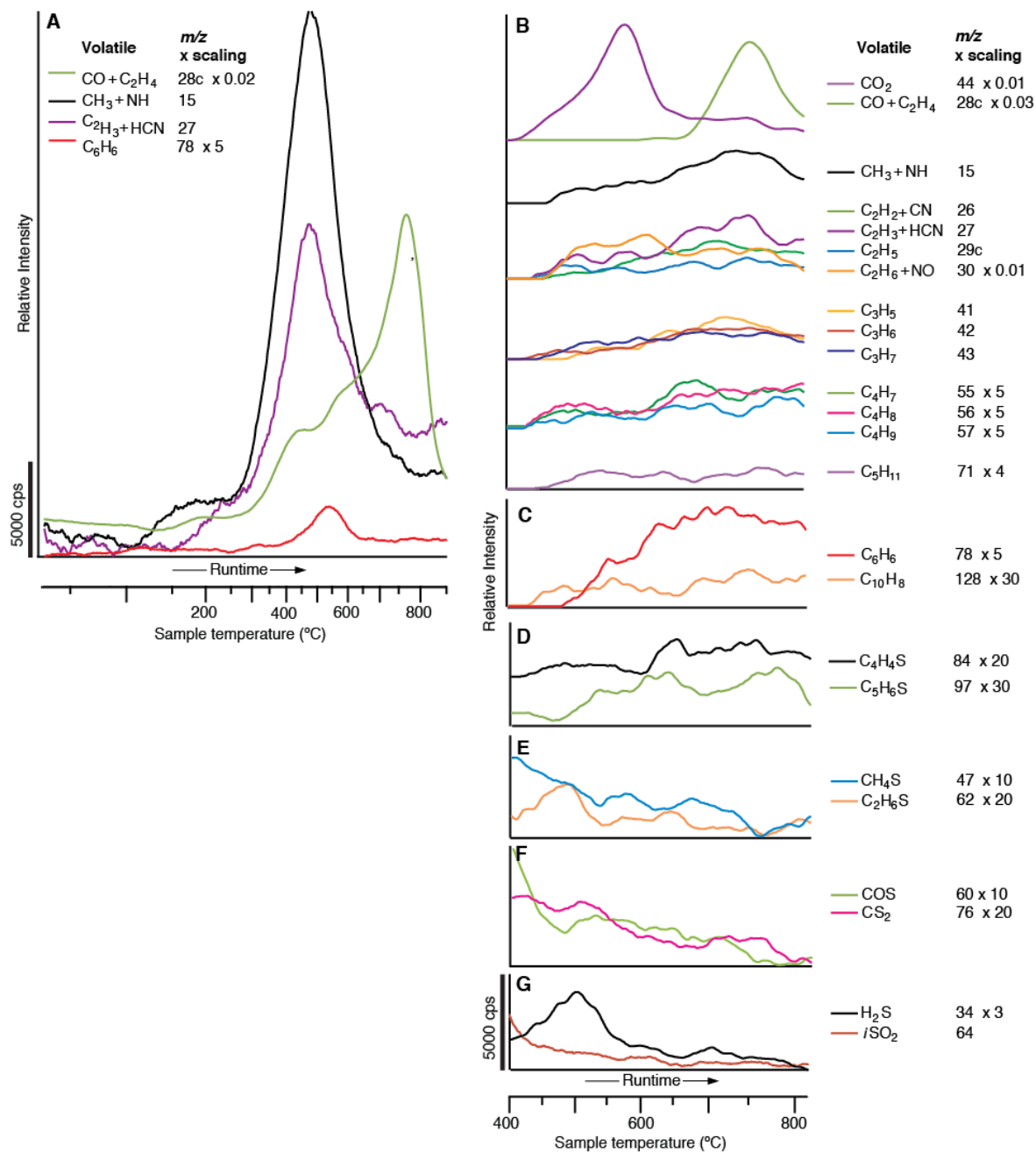
Fig. S9. Evolved gas analysis of the Murchison carbonaceous chondrite on the SAM testbed using the same analytical conditions as the Mojave analysis. The Murchison carbonaceous chondrite is used as a proxy for interplanetary dust particle composition (*53*). A) Most mass profiles show thermal desorption and the main pyrolysis products being released 675°C, however the profiles do not return to background levels. B) Baseline subtraction of the main pyrolysis component allows for a closer examination of the >675°C signals. While there are few discrete peaks, the mass profiles show a stead release that increases with temperature for aliphatic, aromatic, and thiophenic components. Such profiles reflect a steady degradation of macromolecular carbon that makes up the bulk of organic carbon in the Murchison (*14, 54*). Legend in B shows *m/z* value, scaling factor, and related volatile (if known). Values of *m/z* marked with a "c" designate corrections to the profile for interferences of other volatile contributions (*11*). Formulas marked that start with an "*i*" indicate a minor isotopologue. All profiles are background subtracted and on the same scale after applying scaling factor. Profiles in B are shifted along the y-axis to show peaks clearly. X-axis is scaled linearly to runtime to show the changing oven ramp rate and peak areas that scale to abundances. Y-axis scale bar in counts per second (cps) is for all panes. Profiles within panes are multiplied by scaling factors.

26
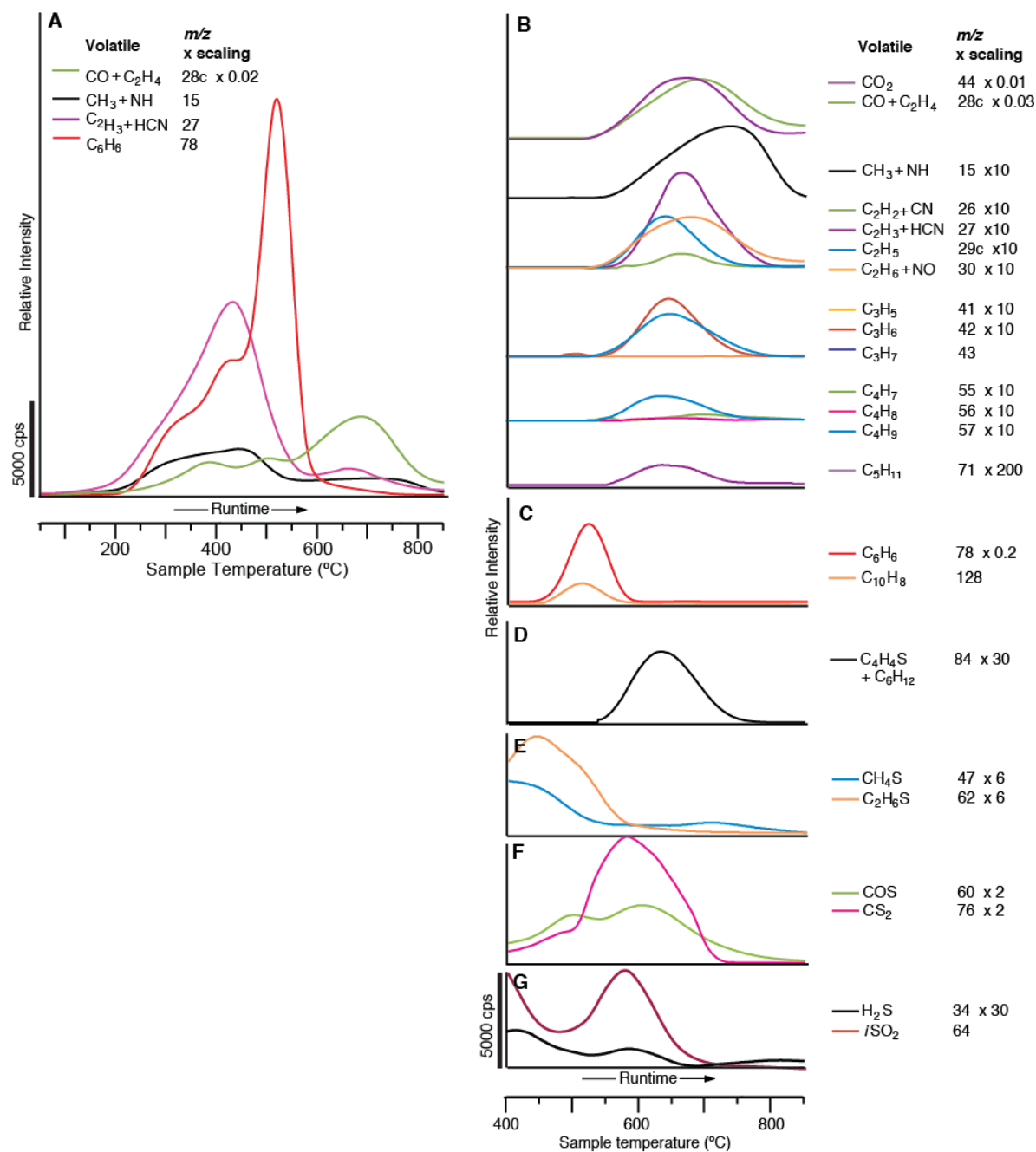
Fig. S10. Evolved gas analysis of the Tissint basaltic martian meteorite in the laboratory using conventional (non-SAM-like) analytical conditions (i.e. 1 bar He, 15 ml/min, 300°C transfer lines). A) Most mass profiles show thermal desorption and the main pyrolysis products being released 550°C, however the profiles do not return to background levels. B) Baseline subtraction of the main pyrolysis component allows for a closer examination of the >550°C signals that include several discrete peaks. One to two ringed aromatics peak at 525°C. Aliphatic compounds (up to C5) and thiophene peak at 650°C. The separate peak evolution for the correlated masses of each molecular group strongly suggest a separate organic phase, likely of macromolecular nature but perhaps retained by minerals at high temperatures (*55*). Legend in B shows *m/z* value, scaling factor, and related volatile (if known). Values of *m/z* marked with a "c" designate corrections to the profile for interferences of other volatile contributions (*10*). Formulas marked that start with an "*i*" indicate a minor isotopologue. All profiles are background subtracted and on the same scale after applying scaling factor. Profiles in B are grouped by carbon number and shifted along the y-axis to show peaks clearly. Profiles in D are similarly shifted. X-axis is scaled linearly to runtime to show the changing oven ramp rate and peak areas that scale to abundances. Y-axis scale bar in counts per second (cps) is for all panes. Profiles within panes are multiplied by scaling factors.

27
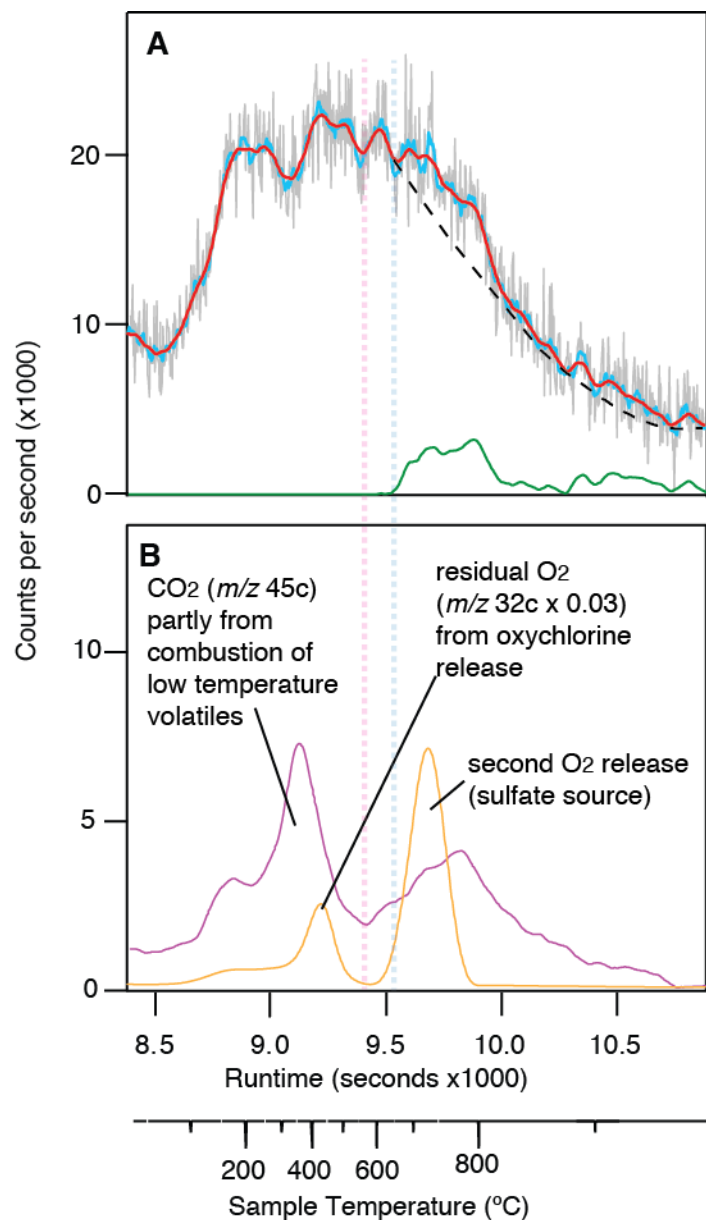
Fig. S11. An example of baseline subtraction for the >400C portion of the data. The Mojave EGA *m/z* 43 profile is used for example. In A, data (no smoothing; gray) is smoothed using a moving average over 11 points (blue). A second smoothing over 21 points effectively removes a majority of residual noise (red). Next, the CO_2 and O_2 profiles in B are used to ascertain the timing of combustion in order to predict whether there are possible residual MTBSTFA products evolving after combustion. The vertical dashed pale pink line indicates the end of oxychlorine-derived O_2 release. The vertical dashed pale blue line indicates the suspected end of post-combustion release of MTBSTFA products and it is used to define the start of the user-defined baseline (dashed black line). This baseline is drawn to make a conservative estimate of other analyte contributions is subtracted. The result is shown in green in pane A. Baseline subtraction was applied to aliphatic, aromatic, and thiophenic compounds.

Table S1. EGA organic carbon abundance estimates for signals above 500ºC (nanomole carbon).*†

Geological Unit	Sample	Thiophene	err	Methylthiophenes	err	Benzene	err	Toluene	err	Benzoic Acid	err	Total Thiophenes	err	Total Aromatics	err
Sheepbed member mudstone	JK-4	0.40	0.21	0.39	0.18	1.18	0.68	1.84	0.79	1.35	0.77	0.79	0.28	4.37	1.29
	CB- Blank1	0.16	0.08	0.25	0.12	1.12	0.21	0.57	0.24	1.02	0.58	0.41	0.15	2.71	0.66
	CB-6	0.21	0.11	0.12	0.06	0.37	0.23	0.61	0.26	0.28	0.16	0.33	0.12	1.26	0.38
	CB-6r	0.10	0.05	0.09	0.04	0.17	0.14	0.38	0.16	0.30	0.17	0.19	0.07	0.86	0.28
	CB-7	0.16	0.08	0.09	0.04	0.26	0.12	0.33	0.14	0.39	0.22	0.24	0.09	0.97	0.29
	CB-Blank2	0.32	0.17	0.16	0.08	0.43	0.15	0.41	0.18	0.48	0.28	0.48	0.19	1.33	0.36
Murray formation mudstone	CH-Blank	0.27	0.15	0.22	0.11	0.94	0.34	0.91	0.40	1.19	0.69	0.49	0.18	3.04	0.86
	CH	1.48	0.79	0.54	0.26	3.12	1.24	3.32	1.44	1.59	0.91	2.02	0.84	8.03	2.11
	MJ	1.66	0.89	0.54	0.26	2.12	1.03	2.76	1.20	2.11	1.21	2.20	0.93	6.99	1.99
	TP	0.41	0.22	0.29	0.14	0.74	0.46	1.24	0.54	0.85	0.49	0.70	0.26	2.82	0.86
	BK	0.43	0.23	0.20	0.10	0.90	0.51	1.36	0.59	0.96	0.55	0.63	0.25	3.22	0.95

Table S1 continued.

Geological Unit	Sample	Methanethiol	err	Dimethylsulfide	err	Carbonyl Sulfide	err	Carbon Disulfide	err	Total C1+C2 Sulfur Compounds	err
Sheepbed member mudstone	JK-4	1.02	0.39	0.84	0.64	1.11	0.43	0.25	0.09	3.21	0.87
	CB- Blank1	0.25	0.10	0.29	0.22	0.15	0.06	0.16	0.06	0.85	0.25
	CB-6	0.73	0.28	0.43	0.33	0.82	0.31	0.05	0.02	2.02	0.53
	CB-6r	0.13	0.05	0.19	0.14	0.07	0.03	0.04	0.01	0.43	0.15
	CB-7	0.41	0.16	0.27	0.21	0.59	0.23	0.06	0.02	1.33	0.34
	CB-Blank2	0.21	0.08	0.22	0.17	0.23	0.09	0.12	0.04	0.77	0.21
Murray formation mudstone	CH-Blank	0.47	0.18	0.43	0.32	0.50	0.20	0.10	0.04	1.49	0.42
	CH	13.6	5.33	5.32	4.05	9.18	3.60	1.25	0.46	29.3	7.61
	MJ	23.4	9.18	6.93	5.27	11.9	4.67	1.54	0.57	43.8	11.6
	TP	8.82	3.46	4.63	3.52	5.69	2.23	0.88	0.32	20.0	5.43
	BK	8.25	3.24	2.74	2.08	4.68	1.84	0.61	0.22	16.3	4.27

Table S1 continued.

Geological Unit	Sample	Total Aliphatic Compounds	err	Total Organic C in Thiophenes, Aromatics, Aliphatic Compounds	err	Total Organic C in Thiophenes, Aromatics, Aliphatic, and C1+C2 Sulfur Compounds	err
Sheepbed member mudstone	JK-4	14.4	2.01	19.6	2.41	22.8	2.56
	CB- Blank1	3.17	0.44	6.28	0.81	7.14	0.85
	CB-6	17.3	2.16	18.9	2.20	20.9	2.26
	CB-6r	5.22	0.66	6.27	0.71	6.70	0.73
	CB-7	22.4	2.76	23.7	2.78	25.0	2.80
	CB-Blank2	1.61	0.21	3.42	0.46	4.19	0.50
Murray formation mudstone	CH-Blank	5.35	0.83	8.88	1.21	10.4	1.28
	CH	20.8	2.79	30.8	3.60	60.2	8.42
	MJ	38.4	5.63	47.6	6.04	91.4	13.1
	TP	9.51	1.28	13.0	1.56	33.1	5.65
	BK	19.0	3.50	22.8	3.64	39.1	5.61

* All estimates assume the identification ion (corrected if applicable) (Fig. 1-2) solely reflects the molecule estimated. Benzoic acid is assumed for *m/z* 105.

† Abundances are normalized to a single portion.

Err = Propagated error from mean +/- 1σ standard deviations, N ≥3.

Table S2. SAM GCMS abundances of methanethiol, dimethylsulfide $(CH_3)_2$, 2-methylthiophene and 3-methylthiophene (C_5H_6S).

Geological Unit	Sample	GC Cut * (°C)	GC molecular detections (picomole) †				
			Methanethiol	**Dimethylsulfide**	**Thiophene**	**2-Methylthiophene**	**3-Methylthiophene**
Sheepbed member mudstone	JK-4	578°-801°	< 1	10 ± 3	10 ± 3	< 1	< 1
	CB-Blank1	447°-558º	11 ± 3	22 ± 6	3 ± 1	< 1	< 1
	CB-6	232°-372º	5 ± 1	36 ± 9	< 2	< 1	< 1
	CB-6r	232°-372º	< 1	13 ± 3	< 2	< 1	< 1
	CB-7	497°-805°	207 ± 50	351 ± 92	6 ± 1	< 1	< 1
	CB-Blank2	497°-805º	< 1	24 ± 6	6 ± 2	< 1	< 1
Murray formation mudstone	CH-Blank	212°-862º	39 ± 10	23 ± 6	< 2	< 1	< 1
	CH	215°-862º	ND ‡	43 ± 11	10 ± 3	< 1	< 1
	MJ	226°-862º	ND ‡	36 ± 10	20 ± 5	5 ± 2	4 ± 1
	TP	GCMS not implemented					
	BK	GCMS did not complete					

* Gas chromatography (GC) hydrocarbon trap cut refers to the cup temperature range over which volatiles were collected on the hydrocarbon trap during pyrolysis for GCMS analyses.

† Abundances are normalized to a single aliquot of sample. Propagated error from mean +/- 1σ standard deviations, N ≥3.

‡ ND: Not determined. In some instances, the compound is present, however, a GC coelution with another compound prevents its quantification.

Table S3. Comparison of GC retention time for analytical standards run on the SAM GC breadboard and the molecules detected in the MJ experiment by SAM.

Compound	Retention Time (min) Laboratory Spare GC-5	Retention Time (min) SAM GC-5 *
Non-retained compound †	3.0	3.0
Ethanethiol	3.6	N/A
Dimethyl Sulfide	3.8	3.7
Propanethiol	4.8	N/A
Thiophene	6.1	6.2
2-Methylthiophene	9.4	9.2
3-Methylthiophene	9.7	9.5
2,5-Dimethylthiophene	12.2	11.9 ‡
Naphthalene	19.4	15.9 §

* Laboratory spare GC5 temperature program: 40°C for 5 min then ramped at 10°C/min to 190°C.

† Non-retained compound is solvent in the laboratory analysis and CO_2 in the SAM MJ analysis.

‡ Signal-to-noise ratio for a possible peak is less than 3.

§ A small peak is present in the *m/z* 128 ion chromatogram of Mojave; however, its retention time does not match that of naphthalene determined on the laboratory spare GC5 possible due to differences in instrument condition following a second heating of the injection trap on the flight system. The laboratory test did not invoke a second injection trap heating.

Table S4. EGA molecular abundance (nanomole S) estimates for sulfur volatiles evolved above 500ºC. *†‡

Geological Unit	Sample	Dihydrogen Sulfide	err	Sulfur Dioxide	err	Total Organic-Sulfur	err	Total Sulfide	err
Sheepbed member mudstone	JK-4	53.6	20.6	624	240	4.45	0.67	58.0	20.6
	CB- Blank1	19.9	7.68	6.86	2.64	1.63	0.17	21.6	7.68
	CB-6	28.8	11.1	1033	398	2.49	0.45	31.3	11.1
	CB-6r	2.90	1.12	11.8	4.53	0.73	0.09	3.64	1.12
	CB-7	32.9	12.7	820	316	1.68	0.29	34.6	12.7
	CB-Blank2	1.47	0.57	9.18	3.54	1.50	0.16	2.98	0.59
Murray formation mudstone	CH-Blank	3.65	1.43	27.2	10.7	2.23	0.32	5.88	1.47
	CH	169	66.4	18562	7279	33.0	6.76	202	66.7
	MJ	233	91.7	14946	5861	48.0	10.6	282	92.3
	TP	132	51.8	7149	2803	21.9	4.49	155	52.0
	BK	86.9	34.1	9651	3784	17.8	3.87	105	34.3

* All estimates assume the identification ion (corrected if applicable) (Fig. 1-2) reflects the molecule estimated.

† Abundances are normalized to a single portion.

‡ Err = Propagated error from mean +/- 1σ standard deviations, N ≥3.

Table S5. Known MTBSTFA and DMF reaction products, the most abundant mass fragments in their NIST mass spectra, and diagnostic ions used for their identification (underlined).

Compound	Abbreviation	Formula	M/z (% of base peak)	Comments on presence in SAM observations
Bisilylated water (disiloxane, 1,3-bis (1,1-dimethylethyl), 1,1,3,3-tetramethyl)	BSW	$C_{12}H_{30}OSi_2$	<u>147</u>, 189(17), 148(16), 73(13), 117(8), 149(8), 133(7)	Always
Monosilylated water (*tert*-butyldimethylsilanol)	MSW	$C_6H_{16}OSi$	<u>75</u>, 76(0.8), 77 (0.4)	Always
tert-butyldimethylsilyl fluoride (or *tert*-butyldimethylfluorosilane)	TBDMS-F	$C_6H_{15}FSi$	<u>77</u>, 55(92), <u>134</u>(18), 78(8)	Always
tert-butyldimethylsilyl chloride (or *tert*-butlydimethylchlorosilane)	TBDMS-Cl	$C_6H_{15}ClSi$	<u>93</u>, 56 (92), 57 (50), <u>95</u> (36), 41 (30), 65, 29 (17), 63, 94, 39 (10), …, 79, 78 (4)	Occasional
Difluorodimethylsilane		$C_2H_6F_2Si$	<u>81</u>, 47 (21), 96, 15 (9), 77 (6)	Possible
Dichlorodimethylsilane		$C_2H_6Cl_2Si$	<u>113</u>, <u>115</u> (70), 63, 65, 117, 93, 15 (10), 128 (7)	Possible
2,2,2-Trifluoro-N-methylacetamide	TFMA	$C_3H_4F_3NO$	<u>58</u>, 69, <u>127</u> (24), 15 (23), 28, 78 (11), …, 106 (2), 30, 97 (2), 128 (2)	Always
Trifluoroacetamide §		$C_2H_2F_3NO$	44, <u>69</u> (14), <u>51</u>(13), …, 113 (1)	Often
Trifluoroacetonitrile		C_2F_3N	<u>69</u>, <u>76</u>(47), 50(25), 31, 12, 26, 38, 14, 19, 95, 24, 57(1), 77(1)	Often
Hydrogen cyanide	HCN	CHN	<u>27</u>, <u>26</u>(17)	Always
Cyanogen chloride	CNCl	CNCl	<u>61</u>, <u>63</u>(32), 35(11), 26(8)	Occasional
Cyanogen bromide	CNBr	CNBr	<u>105</u>, <u>107</u>(95) 79(7), 53(7), 81(7), 54(6), 26(2)	Occasional
Cyanogen		C_2N_2	<u>52</u>, 26(5), 53(3)	Possible, difficult to confirm in EGA
Acetamide		C_2H_5NO	59, 44(99), 43(60), 42(31), 28(8), 41(7), 15(7)	Possible, difficult to confirm in EGA
Nitromethane		CH_3NO_2	30, 61(57), 15(48), 46(37), 29(11), 27(10)	Possible, difficult to confirm in EGA
Methyl isocyanate		C_2H_3NO	57, 28(38), 56(37), 27(15), 55(8), 29(7)	Possible, difficult to confirm in EGA

Table S5 continued.

Compound	Abbreviation	Formula	*M/z* (% of base peak)	Comments on presence in SAM observations
Acetonitrile		C_2H_3N	41, 40(50), 39(18) 38(9), 14(5)	Possible, difficult to confirm in EGA
Acetone		C_3H_6O	43, 58(25), 15(12), 42(10), 27(7), 26(5), 39(5)	Possible, difficult to confirm in EGA
Acetylaldehyde		C_2H_4O	29, 44(83), 43(47), 15(36), 42(13), 14(11)	Possible, difficult to confirm in EGA
2-Methylpropene	MePr	C_4H_8	<u>41</u>, 39(45), <u>56</u>(45), 28(22), 27(22), 55(16), 29(11)	Pyrolysis products, always detected in SAM data
2-Chloro-2-methylpropane	2CMePr	C_4H_9Cl	<u>57</u>, 41(52), <u>77</u>(40), 39(16), <u>79</u>(11), 29(10), 56(6), 27(5), 55(5), 49, 58(4), 76(4)	Possible, difficult to confirm in EGA
1-Chloro-2-methylpropene	1CMePr	C_4H_7Cl	<u>55</u>, 39(48), <u>90</u>(41), <u>53</u>(28), 27(23), 54, 29(20), 41(17), 75, <u>92</u>(13), 62, 77(6), …, 91(3)	Possible, difficult to confirm in EGA (indistinguishable from 3-Chloro-2-methylpropene)
3-Chloro-2-methylpropene	3CMePr	C_4H_7Cl	<u>55</u>, 39(45), <u>90</u>(32), 54(27), 29(23), 27(20), 41(19), 53,75, <u>92</u>(10), 28(6), 50, 40, 38, 51, 56(5), 62, 26, 49, 77(3), …, 91(2)	Possible, difficult to confirm in EGA (indistinguishable from 1-Chloro-2-methylpropene)
Propene	Pr	C_3H_6	<u>41</u>, 39(72), <u>42</u>(70), 27(38), 40, 38, 37, 26(11)	Possible, difficult to confirm in EGA
Chloromethane	CM	CH_3Cl	50, 15(72), <u>52</u>(31), 49(11)	Always
Dichloromethane	DCM	CH_2Cl_2	49, <u>84</u>(65), <u>86</u>(43), 51(32)	Always
Trichloromethane	TriCM	$CHCl_3$	<u>83</u>, <u>85</u>(71), 47(27), 48(13) <u>87</u>(13), …, 82(5)	Occasional
Tetrachloromethane	TetraCM	CCl_4	<u>117</u>, <u>119</u>(96), <u>121</u>(35), 82(24), 47(20), 84(16)	Occasional
Bromomethane	BM	CH_3Br	94, 96(94), 15(47), 93(21), 95(15), 91(7), 79(6)	Occasional
Dibromomethane	DBM	CH_2Br_2	174, <u>93</u>(96), <u>95</u>(85), 172(51), 176(47), <u>81</u>(12), 79(12), 91(11), 94, 92(5)	Possible
Dimethylformamide	DMF	C_3H_7NO	<u>73</u>	Possible, difficult to confirm in EGA, not detected in GC
Carbon dioxide	CO_2	CO_2	<u>44</u>, <u>28</u>(10), <u>16</u>(10), <u>12</u>(9)	Possible, difficult to confirm
Carbon monoxide	CO	CO	<u>28</u>, …, 29(1)	Always
Nitric oxide	NO	NO	<u>30</u>, 14(8), 15(2), 16(2)	Always (indistinguishable from N_2O)
Nitrous oxide	N_2O	N_2O	44, <u>30</u>(31), 14(13), 28(11)	Possible

Table S6. Analytical conditions for SAM analyses.

Geological Unit	Sample	Mass (mg, 2σ SD)*	TID†	Analysis sol	Oven used	GC used	SMS flush/ pump/vent (min)	Pre- delivery sample cup temp. § (C)	Sample preheat temp. § (C)	Preheat hold (min)	Pyrolysis final temp. § (C)
Sheepbed member mudstone	JK-4	45 ± 18	25077	227	1	5	NA ‡	NA ‡	35°-50°	31	882°
	CB-Blank1	0	25083	277	1	5	NA ‡	NA ‡	35°-50°	31	879°
	CB6	135 ± 31	25130	382	1	5	360	≤249°	249°	31	866°
	CB6r	0	25133	394	1	5	360	≤249°	249°	31	866°
	CB-7	135 ± 31	25142	408	1	5	360	≤249°	249°	31	866°
	CB-Blank2	0	25145	421	1	5	360	≤249°	249°	31	866°
Murray formation mudstone	CH-Blank	0	25223	770	2	5	NA ‡	NA ‡	~40°	21	862°
	CH	45 ± 18	25226	773	2	5	NA ‡	NA ‡	~40°	21	862°
	MJ	45 ± 18	25242	887 (EGA) 981 (GC)	2	5	NA ‡	NA ‡	~40°	21	862°
	TP	45 ± 18	25257	928	2	NA ‡	NA ‡	NA ‡	~40°	5	862°
	BK	135 ± 31	25282	1075	2	NA ‡	NA ‡	NA ‡	~40°	21	862°

* Error = mean +/- 2σ standard deviations based on extensive testing using the MSL Drill testbed on different rock samples.

†SAM test identification (TID) number for looking up raw data in the NASA Planetary Data System.

§The sample temperatures for oven 1 were determined from thermocouple measurements of fused silica powder heated in a SAM flight spare oven using the same power profile as the SAM flight oven. These data are recent and may thus differ from temperatures published in previous manuscript. The sample temperatures for oven 2 are based on pre-flight thermal measurements.

‡ NA: Not Applicable.

Table S7. Electron-impact total and partial ionization cross-sections at 70 eV.

Molecule (M)	TICS(M) (Å²)	TICS error (Å²)	TICS source	Ion *m/z*	PICS(ion) (Å²)	PICS error (Å²)	PICS source
Carbon dioxide *	3.57*	0.43	(*56*)	44	2.30	0.28	(*56*)
Carbon monoxide	2.52	0.38	(*48*)	28	0.97	0.19	(*48*)
Methanethiol	7.5	1.13	Calculated by K. Irikura	47	2.55	0.51	Calculated using NIST RMR
Dimethylsulfide	10.86	1.30 †	(*57*)	62	1.66	1.13 †	(*57*)
Carbonyl sulfide	4.93	0.74	(*48*)	60	2.60	0.52	Calculated using NIST RMR
Carbon disulfide	7.97	1.20	(*48*)	76	4.38	0.64	Calculated using NIST RMR
Hydrogen disulfide	4.7	0.71	Calculated by K. Irikura	34	2.43	0.49	Calculated using NIST RMR
Thiophene	13.60	1.63 †	(*57*)	84	2.32	1.47 †	(*57*)
2-Methylthiophene	16.97	2.04 †	(*57*)	97	3.61	1.95 †	(*57*)
3-Methylthiophene	16.98	2.04 †	(*57*)	97	3.88	1.93 †	(*7*)
Average of methylthiophenes isomers	15.28	2.38		97	2.96	1.94	
Benzo(a)thiophene	23.66	2.84 †	(*57*)	134	7.63	1.87 †	(*57*)
Benzene (C_6H_6)	15.52	1.86 †	(*57*)	78	3.93	1.17 †	(*57*)
Toluene	18.48	2.22 †	(*57*)	91	5.29	1.45 †	(*57*)
Benzoic acid	19.13	2.30 †	(*57*)	105	2.90	1.35 †	(*57*)
Methane (CH_4)	3.52	0.53	(*48*)	16	1.48	0.01	Calculated by K. Irikura
Ethane (C_2H_6)	6.42	0.96	(*48*)	30	0.77	0.02	Calculated by K. Irikura
Propane ($C3H_8$)	8.62	1.29	(*48*)	29	2.64	0.53	Calculated using NIST RMR
Ethene (C_2H4)	5.12	0.77	(*48*)	27	1.38	0.28	Calculated using NIST RMR
Propene (C_3H_6)	8.74	1.31	(*48*)	41	0.30	0.05	(*58*)
1-Butene † (C_4H_8)	11.79	1.77	(*48*)	56	1.49	0.30	Calculated using NIST RMR
2-Butene (C_4H_8)	4.14	0.62	(*48*)	56	0.48	0.10	Calculated using NIST RMR

* ICSs for CO_2 from Tian et al. (*56*) are deemed the most accurate measurement (K. Irikura, personal communication).

† Uncertainties for BEB-calculated PICSs are calculated mean +/- 1σ standard deviations (N ≥10), assuming a normal distribution.

Table S8. EGA molecular abundance estimates for signals above 500ºC (nanomole molecule). *†

Geological Unit	Sample	Thiophene	err	Methyl-thiophenes	err	Benzene	err	Toluene	err	Benzoic Acid	err	Total Thiophenes	err	Total Aromatics	err
Sheepbed member mudstone	JK-4	0.10	0.05	0.08	0.04	0.20	0.11	0.26	0.11	0.19	0.11	0.18	0.06	0.65	0.19
	CB- Blank1	0.04	0.02	0.05	0.02	0.19	0.03	0.08	0.03	0.15	0.08	0.09	0.03	0.41	0.10
	CB-6	0.05	0.03	0.02	0.01	0.06	0.04	0.09	0.04	0.04	0.02	0.08	0.03	0.19	0.06
	CB-6r	0.03	0.01	0.02	0.01	0.03	0.02	0.05	0.02	0.04	0.02	0.04	0.02	0.13	0.04
	CB-7	0.04	0.02	0.02	0.01	0.04	0.02	0.05	0.02	0.06	0.03	0.06	0.02	0.15	0.04
	CB-Blank2	0.08	0.04	0.03	0.02	0.07	0.03	0.06	0.03	0.07	0.04	0.11	0.05	0.20	0.05
Murray formation mudstone	CH-Blank	0.07	0.04	0.04	0.02	0.16	0.06	0.13	0.06	0.17	0.10	0.11	0.04	0.46	0.13
	CH	0.37	0.20	0.11	0.05	0.52	0.21	0.47	0.21	0.23	0.13	0.48	0.21	1.22	0.32
	MJ	0.42	0.22	0.11	0.05	0.35	0.17	0.39	0.17	0.30	0.17	0.52	0.23	1.05	0.30
	TP	0.10	0.06	0.06	0.03	0.12	0.08	0.18	0.08	0.12	0.07	0.16	0.06	0.42	0.13
	BK	0.11	0.06	0.04	0.02	0.15	0.08	0.19	0.08	0.14	0.08	0.15	0.06	0.48	0.14

Table S8 continued.

Geological Unit	Sample	Methane-thiol	err	Dimethyl-sulfide	err	Carbonyl Sulfide	err	Carbon Disulfide	err	Total C1+C2 Sulfur Compounds	err
Sheepbed member mudstone	JK-4	1.02	0.39	0.42	0.32	1.11	0.43	0.25	0.09	2.79	0.67
	CB- Blank1	0.25	0.10	0.15	0.11	0.15	0.06	0.16	0.06	0.70	0.17
	CB-6	0.73	0.28	0.22	0.16	0.82	0.31	0.05	0.02	1.81	0.45
	CB-6r	0.13	0.05	0.09	0.07	0.07	0.03	0.04	0.01	0.33	0.09
	CB-7	0.41	0.16	0.14	0.10	0.59	0.23	0.06	0.02	1.19	0.29
	CB-Blank2	0.21	0.08	0.11	0.08	0.23	0.09	0.12	0.04	0.66	0.15
Murray formation mudstone	CH-Blank	0.47	0.18	0.21	0.16	0.50	0.20	0.10	0.04	1.28	0.32
	CH	13.6	5.33	2.66	2.02	9.18	3.60	1.25	0.46	26.7	6.76
	MJ	23.4	9.18	3.46	2.63	11.9	4.67	1.54	0.57	40.3	10.6
	TP	8.82	3.46	2.32	1.76	5.69	2.23	0.88	0.32	17.71	4.49
	BK	8.25	3.24	1.37	1.04	4.68	1.84	0.61	0.22	14.91	3.87

* All estimates assume the identification ion (corrected if applicable) (Fig. 1-2) solely reflects the molecule estimated. Benzoic acid is assumed for *m/z* 105.

† Abundances are normalized to a single portion.

Err = Propagated error from mean +/- 1σ standard deviations, N ≥3.

Table S9. EGA molecular concentration estimates for signals above 500ºC (parts per billion molecules by mass). *†‡

Geological Unit	Sample	Thiophene	err	Methyl-thiophenes	err	Benzene	err	Toluene	err	Benzoic Acid	err	Total Thiophenes	err	Total Aromatics	err
Sheepbed member mudstone	JK-4	186	109	170	90	340	212	538	264	525	325	356	141	1400	469
	CB- Blank1	73	43	109	58	324	99	167	82	395	245	182	72	886	276
	CB-6	98	57	51	27	106	70	179	88	108	67	149	63	393	131
	CB-6r	47	28	37	20	50	42	111	54	118	73	85	34	279	100
	CB-7	73	43	37	20	75	39	95	47	150	93	110	47	321	111
	CB-Blank2	149	87	71	38	124	53	121	59	188	116	220	95	433	141
Murray formation mudstone	CH-Blank	128	75	97	52	273	118	266	132	462	288	224	91	1000	338
	CH	692	407	237	127	903	418	971	482	616	384	929	426	2490	745
	MJ	777	457	236	127	614	332	807	401	818	510	1013	474	2240	729
	TP	193	114	126	68	214	143	362	180	329	205	319	132	904	308
	BK	199	117	88	47	261	159	397	197	372	232	287	126	1030	343

Table S9 continued.

Geological Unit	Sample	Methane-thiol	err	Dimethyl-sulfide	err	Carbonyl Sulfide	err	Carbon Disulfide	err	Total C1+C2 Sulfur Compounds	err
Sheepbed member mudstone	JK-4	1090	494	580	461	1480	670	415	179	3560	969
	CB- Blank1	268	122	202	160	203	92	263	114	936	249
	CB-6	775	352	298	237	1090	495	82	36	2250	653
	CB-6r	135	61	131	104	98	45	67	29	431	132
	CB-7	437	198	187	149	783	355	101	44	1510	435
	CB-Blank2	223	101	152	121	302	137	195	85	872	225
Murray formation mudstone	CH-Blank	501	230	294	235	668	307	163	72	1627	456
	CH	14500	6680	3670	2930	12300	5640	2120	928	32600	9260
	MJ	25000	11500	4780	3810	15900	7310	2610	1150	48300	14200
	TP	9430	4340	3200	2550	7600	3490	1500	656	21700	6160
	BK	8820	4060	1890	1510	6250	2870	1040	454	18000	5210

* All estimates assume the identification ion (corrected if applicable) (Fig. 1-2) reflects the molecule estimated. Benzoic acid is assumed for *m/z* 105.

† Abundances are normalized to a single portion.

Err = Propagated error from mean +/- 1σ standard deviations, N ≥3.

Table S10. EGA organic carbon concentration estimates for signals above 500ºC (parts per billion C by mass, unless noted ppm C). *†‡

Geological Unit	Sample	Thiophene	err	Methyl-thiophenes	err	Benzene	err	Toluene	err	Benzoic Acid	err	Total thiophenes	err	Total aromatics	err
Sheepbed member mudstone	JK-4	106	62.0	104	55.2	314	195	491	241	361	224	210	83.0	1166	382
	CB- Blank1	41.9	24.5	66.7	35.5	299	91.0	152	74.7	272	168	109	43.1	723	206
	CB-6	56.0	32.7	31.0	16.5	97.8	64.5	164	80.3	74.4	46.1	87.0	36.6	336	113
	CB-6r	27.0	15.8	22.9	12.2	46.3	38.7	101	49.6	81.2	50.2	49.9	19.9	229	80.5
	CB-7	41.7	24.3	22.8	12.1	69.4	36.1	87.0	42.8	103	64.0	64.5	27.2	260	85.0
	CB-Blank2	85.0	49.6	43.5	23.1	114	49.0	111	54.3	129	80.0	129	54.7	354	108
Murray formation mudstone	CH-Blank	72.8	42.8	59.3	31.8	252	109	242	120	318	198	132	53.4	812	256
	CH	395	232	145	77.9	833	386	886	440	424	265	540	245	2140	642
	MJ	444	261	144	77.5	566	306	736	366	563	351	588	272	1870	592
	TP	110	64.9	77.2	41.4	198	132	330	164	226	141	188	77.0	754	253
	BK	114	66.9	53.9	29.0	241	147	362	180	256	160	168	72.9	859	282

Table S10 continued.

Geological Unit	Sample	Methanethiol	err	Dimethylsulfide	err	Carbonyl Sulfide	err	Carbon Disulfide	err	Total C1+C2 Sulfur Compounds	err	Total Aliphatic Compounds	err
Sheepbed member mudstone	JK-4	272	123	224	178.	295.	134	65.5	28.3	857	256	3860	925
	CB- Blank1	66.9	30.3	77.9	61.9	40.7	18.5	41.5	17.9	227	74	846	195
	CB-6	194	87.8	115	91.6	218.	99.0	13.0	5.6	540	161	4620	1020
	CB-6r	33.7	15.3	50.7	40.2	19.6	8.9	10.6	4.6	115	44.2	1390	175
	CB-7	109	49.5	72.3	57.4	156.	71.0	15.9	6.9	354	104	5990	737
	CB-Blank2	55.6	25.2	58.8	46.7	60.4	27.4	30.8	13.3	206	61.2	431	108
Murray formation mudstone	CH-Blank	125	57.5	113	90.7	133.	61.4	25.7	11.3	398	124	1430	360
	CH	3630	1670	1420	1130	2450	1130	334	146	7830	2310	5540	1230
	MJ	6250	2870	1850	1470	3180	1461	412	181	11700	3550	10200	2350
	TP	2350	1080	1240	986	1520	698	236	104	5350	1630	2540	559
	BK	2200	1010	731	583	1250	574	163	71.7	4350	1300	5060	1310

Table S10 continued.

Geological Unit	Sample	Total Organic C in Thiophenes, Aromatics, Aliphatic Compounds (ppm C)	err	Total Organic C in Thiophenes, Aromatics, Aliphatic, and C1+C2 Sulfur Compounds (ppm C)	err
Sheepbed member mudstone	JK-4	5.23	1.00	6.09	0.26
	CB- Blank1	1.68	0.29	1.90	0.07
	CB-6	5.04	1.03	5.58	0.16
	CB-6r	1.67	0.19	1.79	0.04
	CB-7	6.31	0.74	6.67	0.10
	CB-Blank2	0.91	0.16	1.12	0.06
Murray formation mudstone	CH-Blank	2.37	0.45	2.77	0.12
	CH	8.23	1.41	16.1	2.31
	MJ	12.7	2.44	24.4	3.55
	TP	3.48	0.62	8.83	1.63
	BK	6.09	1.34	10.4	1.30

* All estimates assume the identification ion (corrected if applicable) (Fig. 1-2) reflects the molecule estimated. Benzoic acid is assumed for *m/z* 105.

† Abundances are normalized to a single portion.

‡ Err = Propagated error from mean +/- 1σ standard deviations, N ≥3.

References and Notes

1. C. Freissinet, D. P. Glavin, P. R. Mahaffy, K. E. Miller, J. L. Eigenbrode, R. E. Summons, A. E. Brunner, A. Buch, C. Szopa, P. D. Archer Jr., H. B. Franz, S. K. Atreya, W. B. Brinckerhoff, M. Cabane, P. Coll, P. G. Conrad, D. J. Des Marais, J. P. Dworkin, A. G. Fairén, P. François, J. P. Grotzinger, S. Kashyap, I. L. Ten Kate, L. A. Leshin, C. A. Malespin, M. G. Martin, F. J. Martin-Torres, A. C. McAdam, D. W. Ming, R. Navarro-González, A. A. Pavlov, B. D. Prats, S. W. Squyres, A. Steele, J. C. Stern, D. Y. Sumner, B. Sutter, M.-P. Zorzano, Organic molecules in the Sheepbed mudstone, Gale Crater, Mars. *J. Geophys. Res. Planets* **120**, 495–514 (2015). doi:10.1002/2014JE004737 Medline

2. D. W. Ming, P. D. Archer Jr., D. P. Glavin, J. L. Eigenbrode, H. B. Franz, B. Sutter, A. E. Brunner, J. C. Stern, C. Freissinet, A. C. McAdam, P. R. Mahaffy, M. Cabane, P. Coll, J. L. Campbell, S. K. Atreya, P. B. Niles, J. F. Bell 3rd, D. L. Bish, W. B. Brinckerhoff, A. Buch, P. G. Conrad, D. J. Des Marais, B. L. Ehlmann, A. G. Fairén, K. Farley, G. J. Flesch, P. Francois, R. Gellert, J. A. Grant, J. P. Grotzinger, S. Gupta, K. E. Herkenhoff, J. A. Hurowitz, L. A. Leshin, K. W. Lewis, S. M. McLennan, K. E. Miller, J. Moersch, R. V. Morris, R. Navarro-González, A. A. Pavlov, G. M. Perrett, I. Pradler, S. W. Squyres, R. E. Summons, A. Steele, E. M. Stolper, D. Y. Sumner, C. Szopa, S. Teinturier, M. G. Trainer, A. H. Treiman, D. T. Vaniman, A. R. Vasavada, C. R. Webster, J. J. Wray, R. A. Yingst, MSL Science Team, Volatile and organic compositions of sedimentary rocks in Yellowknife Bay, Gale crater, Mars. *Science* **343**, 1245267 (2014). doi:10.1126/science.1245267 Medline

3. B. Sutter, A. C. McAdam, P. R. Mahaffy, D. W. Ming, K. S. Edgett, E. B. Rampe, J. L. Eigenbrode, H. B. Franz, C. Freissinet, J. P. Grotzinger, A. Steele, C. H. House, P. D. Archer, C. A. Malespin, R. Navarro-González, J. C. Stern, J. F. Bell, F. J. Calef, R. Gellert, D. P. Glavin, L. M. Thompson, A. S. Yen, Evolved gas analyses of sedimentary rocks and eolian sediment in Gale Crater, Mars: Results of the Curiosity rover's sample analysis at Mars instrument from Yellowknife Bay to the Namib Dune. *J. Geophys. Res. Planets* **122**, 2574–2609 (2017). doi:10.1002/2016JE005225

4. R. Navarro-González, E. Vargas, J. de la Rosa, A. C. Raga, C. P. McKay, Reanalysis of the Viking results suggests perchlorate and organics at midlatitudes on Mars. *J. Geophys. Res. Solid Earth* **115** (E12), E12010 (2010). doi:10.1029/2010JE003599

5. A. Steele, F. M. McCubbin, M. D. Fries, The provenance, formation, and implications of reduced carbon phases in Martian meteorites. *Meteorit. Planet. Sci.* **51**, 2203–2225 (2016). doi:10.1111/maps.12670

6. J. P. Grotzinger, S. Gupta, M. C. Malin, D. M. Rubin, J. Schieber, K. Siebach, D. Y. Sumner, K. M. Stack, A. R. Vasavada, R. E. Arvidson, F. Calef 3rd, L. Edgar, W. F. Fischer, J. A. Grant, J. Griffes, L. C. Kah, M. P. Lamb, K. W. Lewis, N. Mangold, M. E. Minitti, M. Palucis, M. Rice, R. M. E. Williams, R. A. Yingst, D. Blake, D. Blaney, P. Conrad, J. Crisp, W. E. Dietrich, G. Dromart, K. S. Edgett, R. C. Ewing, R. Gellert, J. A. Hurowitz, G. Kocurek, P. Mahaffy, M. J. McBride, S. M. McLennan, M. Mischna, D. Ming, R. Milliken, H. Newsom, D. Oehler, T. J. Parker, D. Vaniman, R. C. Wiens, S. A. Wilson,

Deposition, exhumation, and paleoclimate of an ancient lake deposit, Gale crater, Mars. *Science* **350**, aac7575 (2015). doi:10.1126/science.aac7575 Medline

7. E. Rampe, D. W. Ming, D. F. Blake, T. F. Bristow, S. J. Chipera, J. P. Grotzinger, R. V. Morris, S. M. Morrison, D. T. Vaniman, A. S. Yen, C. N. Achilles, P. I. Craig, D. J. Des Marais, R. T. Downs, J. D. Farmer, K. V. Fendrich, R. Gellert, R. M. Hazen, L. C. Kah, J. M. Morookian, T. S. Peretyazhko, P. Sarrazin, A. H. Treiman, J. A. Berger, J. Eigenbrode, A. G. Fairén, O. Forni, S. Gupta, J. A. Hurowitz, N. L. Lanza, M. E. Schmidt, K. Siebach, B. Sutter, L. M. Thompson, Mineralogy of an ancient lacustrine mudstone succession from the Murray formation, Gale crater, Mars. *Earth Planet. Sci. Lett.* **471**, 172–185 (2017). doi:10.1016/j.epsl.2017.04.021

8. J. A. Hurowitz, J. P. Grotzinger, W. W. Fischer, S. M. McLennan, R. E. Milliken, N. Stein, A. R. Vasavada, D. F. Blake, E. Dehouck, J. L. Eigenbrode, A. G. Fairén, J. Frydenvang, R. Gellert, J. A. Grant, S. Gupta, K. E. Herkenhoff, D. W. Ming, E. B. Rampe, M. E. Schmidt, K. L. Siebach, K. Stack-Morgan, D. Y. Sumner, R. C. Wiens, Redox stratification of an ancient lake in Gale crater, Mars. *Science* **356**, eaah6849 (2017). doi:10.1126/science.aah6849 Medline

9. R. E. Summons, J. P. Amend, D. Bish, R. Buick, G. D. Cody, D. J. Des Marais, G. Dromart, J. L. Eigenbrode, A. H. Knoll, D. Y. Sumner, Preservation of martian organic and environmental records: Final report of the Mars biosignature working group. *Astrobiology* **11**, 157–181 (2011). doi:10.1089/ast.2010.0506 Medline

10. P. R. Mahaffy, C. R. Webster, M. Cabane, P. G. Conrad, P. Coll, S. K. Atreya, R. Arvey, M. Barciniak, M. Benna, L. Bleacher, W. B. Brinckerhoff, J. L. Eigenbrode, D. Carignan, M. Cascia, R. A. Chalmers, J. P. Dworkin, T. Errigo, P. Everson, H. Franz, R. Farley, S. Feng, G. Frazier, C. Freissinet, D. P. Glavin, D. N. Harpold, D. Hawk, V. Holmes, C. S. Johnson, A. Jones, P. Jordan, J. Kellogg, J. Lewis, E. Lyness, C. A. Malespin, D. K. Martin, J. Maurer, A. C. McAdam, D. McLennan, T. J. Nolan, M. Noriega, A. A. Pavlov, B. Prats, E. Raaen, O. Sheinman, D. Sheppard, J. Smith, J. C. Stern, F. Tan, M. Trainer, D. W. Ming, R. V. Morris, J. Jones, C. Gundersen, A. Steele, J. Wray, O. Botta, L. A. Leshin, T. Owen, S. Battel, B. M. Jakosky, H. Manning, S. Squyres, R. Navarro-González, C. P. McKay, F. Raulin, R. Sternberg, A. Buch, P. Sorensen, R. Kline-Schoder, D. Coscia, C. Szopa, S. Teinturier, C. Baffes, J. Feldman, G. Flesch, S. Forouhar, R. Garcia, D. Keymeulen, S. Woodward, B. P. Block, K. Arnett, R. Miller, C. Edmonson, S. Gorevan, E. Mumm, The Sample Analysis at Mars investigation and instrument suite. *Space Sci. Rev.* **170**, 401–478 (2012). doi:10.1007/s11214-012-9879-z

11. Materials and methods are available as supplementary materials.

12. S. C. Moldoveanu, *Pyrolysis of Organic Molecules with Applications to Health and Environmental Issues*. S. C. Moldoveanu, Ed., Techniques and Instrumentation in Analytical Chemistry (Elsevier, New York, 2010), vol. 28, pp. 724.

13. S. C. Moldoveanu, *Analytical Pyrolysis of Natural Organic Polymers*. S. C. Moldoveanu, Ed., Techniques and instrumentation in analytical chemistry (Elsevier, New York, 1998), vol. 20, pp. 496.

14. F. Okumura, K. Mimura, Gradual and stepwise pyrolyses of insoluble organic matter from the Murchison meteorite revealing chemical structure and isotopic distribution. *Geochim. Cosmochim. Acta* **75**, 7063–7080 (2011). doi:10.1016/j.gca.2011.09.015

15. L. Remusat, L. S. Derenne, F. Robert, H. Knicker, New pyrolytic and spectroscopic data on Orgueil and Murchison insoluble organic matter: A different origin than soluble? *Geochim. Cosmochim. Acta* **69**, 3919–3932 (2005). doi:10.1016/j.gca.2005.02.032

16. F. W. McLafferty, F. Tureek, *Interpretation of Mass Spectra* (University Science Books, 1993).

17. J. S. Sinninghe Damsté, T. I. Eglinton, J. W. De Leeuw, P. A. Schenck, Organic sulphur in macromolecular sedimentary organic matter: I. Structure and origin of sulphur-containing moieties in kerogen, asphaltenes and coal as revealed by flash pyrolysis. *Geochim. Cosmochim. Acta* **53**, 873–889 (1989). doi:10.1016/0016-7037(89)90032-X

18. B. P. Baruah, P. Khare, Pyrolysis of high sulfur Indian coals. *Energy Fuels* **21**, 3346–3352 (2007). doi:10.1021/ef070005i

19. L. Xu, J. Yang, Y. Li, Z. Liu, Behavior of organic sulfur model compounds in pyrolysis under coal-like environment. *Fuel Process. Technol.* **85**, 1013–1024 (2004). doi:10.1016/j.fuproc.2003.11.036

20. A. C. McAdam, H. B. Franz, B. Sutter, P. D. Archer Jr., C. Freissinet, J. L. Eigenbrode, D. W. Ming, S. K. Atreya, D. L. Bish, D. F. Blake, H. E. Bower, A. Brunner, A. Buch, D. P. Glavin, J. P. Grotzinger, P. R. Mahaffy, S. M. McLennan, R. V. Morris, R. Navarro-González, E. B. Rampe, S. W. Squyres, A. Steele, J. C. Stern, D. Y. Sumner, J. J. Wray, Sulfur-bearing phases detected by evolved gas analysis of the Rocknest aeolian deposit, Gale Crater, Mars. *J. Geophys. Res. Planets* **119**, 373–393 (2014). doi:10.1002/2013JE004518

21. R. F. C. Brown, *Pyrolytic Methods in Organic Chemistry: Application of Flow and Flash Vacuum Pyrolytic Techniques* (Academic Press, 1980).

22. M. Bajus, Sulfur compounds in hydrocarbon pyrolysis. *Sulfur Rep.* **9**, 25–66 (1989).

23. D. M. Hassler, C. Zeitlin, R. F. Wimmer-Schweingruber, B. Ehresmann, S. Rafkin, J. L. Eigenbrode, D. E. Brinza, G. Weigle, S. Böttcher, E. Böhm, S. Burmeister, J. Guo, J. Köhler, C. Martin, G. Reitz, F. A. Cucinotta, M.-H. Kim, D. Grinspoon, M. A. Bullock, A. Posner, J. Gómez-Elvira, A. Vasavada, J. P. Grotzinger, MSL Science Team, Mars' surface radiation environment measured with the Mars Science Laboratory's Curiosity rover. *Science* **343**, 1244797 (2014). doi:10.1126/science.1244797 Medline

24. K. A. Farley, C. Malespin, P. Mahaffy, J. P. Grotzinger, P. M. Vasconcelos, R. E. Milliken, M. Malin, K. S. Edgett, A. A. Pavlov, J. A. Hurowitz, J. A. Grant, H. B. Miller, R. Arvidson, L. Beegle, F. Calef, P. G. Conrad, W. E. Dietrich, J. Eigenbrode, R. Gellert, S. Gupta, V. Hamilton, D. M. Hassler, K. W. Lewis, S. M. McLennan, D. Ming, R. Navarro-González, S. P. Schwenzer, A. Steele, E. M. Stolper, D. Y. Sumner, D. Vaniman, A. Vasavada, K. Williford, R. F. Wimmer-Schweingruber, MSL Science Team, In situ radiometric and exposure age dating of the martian surface. *Science* **343**, 1247166 (2014). doi:10.1126/science.1247166 Medline

25. P. E. Martin, K. A. Farley, M. B. Baker, C. A. Malespin, S. P. Schwenzer, B. A. Cohen, P. R. Mahaffy, A. C. McAdam, D. W. Ming, P. M. Vasconcelos, R. Navarro-González, A two-step K-Ar experiment on Mars: Dating the diagenetic formation of jarosite from Amazonian groundwaters. *J. Geophys. Res. Planets* **122**, 2803–2818 (2017). doi:10.1002/2017JE005445

26. L. Mayer, The inertness of being organic. *Mar. Chem.* **92**, 135–140 (2004). doi:10.1016/j.marchem.2004.06.022

27. G. J. Flynn, L. R. Nittler, C. Engrand, Composition of cosmic dust: Sources and implications for the early solar system. *Elements* **12**, 177–183 (2016). doi:10.2113/gselements.12.3.177

28. R. G. Keil, L. M. Mayer, Mineral matrices and organic matter. *Org. Geochem.* **12**, 337 (2014).

29. D. T. Vaniman, D. L. Bish, D. W. Ming, T. F. Bristow, R. V. Morris, D. F. Blake, S. J. Chipera, S. M. Morrison, A. H. Treiman, E. B. Rampe, M. Rice, C. N. Achilles, J. P. Grotzinger, S. M. McLennan, J. Williams, J. F. Bell 3rd, H. E. Newsom, R. T. Downs, S. Maurice, P. Sarrazin, A. S. Yen, J. M. Morookian, J. D. Farmer, K. Stack, R. E. Milliken, B. L. Ehlmann, D. Y. Sumner, G. Berger, J. A. Crisp, J. A. Hurowitz, R. Anderson, D. J. Des Marais, E. M. Stolper, K. S. Edgett, S. Gupta, N. Spanovich, MSL Science Team, Mineralogy of a mudstone at Yellowknife Bay, Gale crater, Mars. *Science* **343**, 1243480 (2014). doi:10.1126/science.1243480 Medline

30. J. P. Grotzinger, D. Y. Sumner, L. C. Kah, K. Stack, S. Gupta, L. Edgar, D. Rubin, K. Lewis, J. Schieber, N. Mangold, R. Milliken, P. G. Conrad, D. DesMarais, J. Farmer, K. Siebach, F. Calef 3rd, J. Hurowitz, S. M. McLennan, D. Ming, D. Vaniman, J. Crisp, A. Vasavada, K. S. Edgett, M. Malin, D. Blake, R. Gellert, P. Mahaffy, R. C. Wiens, S. Maurice, J. A. Grant, S. Wilson, R. C. Anderson, L. Beegle, R. Arvidson, B. Hallet, R. S. Sletten, M. Rice, J. Bell 3rd, J. Griffes, B. Ehlmann, R. B. Anderson, T. F. Bristow, W. E. Dietrich, G. Dromart, J. Eigenbrode, A. Fraeman, C. Hardgrove, K. Herkenhoff, L. Jandura, G. Kocurek, S. Lee, L. A. Leshin, R. Leveille, D. Limonadi, J. Maki, S. McCloskey, M. Meyer, M. Minitti, H. Newsom, D. Oehler, A. Okon, M. Palucis, T. Parker, S. Rowland, M. Schmidt, S. Squyres, A. Steele, E. Stolper, R. Summons, A. Treiman, R. Williams, A. Yingst, MSL Science Team, A habitable fluvio-lacustrine environment at Yellowknife Bay, Gale crater, Mars. *Science* **343**, 1242777 (2014). doi:10.1126/science.1242777 Medline

31. Y. Hebting, P. Schaeffer, A. Behrens, P. Adam, G. Schmitt, P. Schneckenburger, S. M. Bernasconi, P. Albrecht, Biomarker evidence for a major preservation pathway of sedimentary organic carbon. *Science* **312**, 1627–1631 (2006). doi:10.1126/science.1126372 Medline

32. H. B. Franz, A. C. McAdam, D. W. Ming, C. Freissinet, P. R. Mahaffy, D. L. Eldridge, W. W. Fischer, J. P. Grotzinger, C. H. House, J. A. Hurowitz, S. M. McLennan, S. P. Schwenzer, D. T. Vaniman, P. D. Archer Jr., S. K. Atreya, P. G. Conrad, J. W. Dottin III, J. L. Eigenbrode, K. A. Farley, D. P. Glavin, S. S. Johnson, C. A. Knudson, R. V. Morris, R. Navarro-González, A. A. Pavlov, R. Plummer, E. B. Rampe, J. C. Stern, A. Steele, R.

E. Summons, B. Sutter, Large sulfur isotope fractionations in Martian sediments at Gale crater. *Nat. Geosci.* **10**, 658–662 (2017). doi:10.1038/ngeo3002

33. P. J. Linstrom, W. G. Mallard, Eds., NIST Chemistry WebBook, NIST Standard Reference Database Number 69 (National Institute of Standards and Technology); https://webbook.nist.gov/chemistry/.

34. K. M. Stack, J. P. Grotzinger, L. C. Kah, M. E. Schmidt, N. Mangold, K. S. Edgett, D. Y. Sumner, K. L. Siebach, M. Nachon, R. Lee, D. L. Blaney, L. P. Deflores, L. A. Edgar, A. G. Fairén, L. A. Leshin, S. Maurice, D. Z. Oehler, M. S. Rice, R. C. Wiens, Diagenetic origin of nodules in the Sheepbed member, Yellowknife Bay formation, Gale crater, Mars. *J. Geophys. Res. Planets* **119**, 1637–1664 (2014). doi:10.1002/2014JE004617

35. R. V. Morris, D. T. Vaniman, D. F. Blake, R. Gellert, S. J. Chipera, E. B. Rampe, D. W. Ming, S. M. Morrison, R. T. Downs, A. H. Treiman, A. S. Yen, J. P. Grotzinger, C. N. Achilles, T. F. Bristow, J. A. Crisp, D. J. Des Marais, J. D. Farmer, K. V. Fendrich, J. Frydenvang, T. G. Graff, J.-M. Morookian, E. M. Stolper, S. P. Schwenzer, Silicic volcanism on Mars evidenced by tridymite in high-SiO_2 sedimentary rock at Gale crater. *Proc. Natl. Acad. Sci. U.S.A.* **113**, 7071–7076 (2016). doi:10.1073/pnas.1607098113 Medline

36. T. F. Bristow, D. L. Bish, D. T. Vaniman, R. V. Morris, D. F. Blake, J. P. Grotzinger, E. B. Rampe, J. A. Crisp, C. N. Achilles, D. W. Ming, B. L. Ehlmann, P. L. King, J. C. Bridges, J. L. Eigenbrode, D. Y. Sumner, S. J. Chipera, J. M. Moorokian, A. H. Treiman, S. M. Morrison, R. T. Downs, J. D. Farmer, D. D. Marais, P. Sarrazin, M. M. Floyd, M. A. Mischna, A. C. McAdam, The origin and implications of clay minerals from Yellowknife Bay, Gale crater, Mars. *Am. Mineral.* **100**, 824–836 (2015). doi:10.2138/am-2015-5077CCBYNCND Medline

37. M. Nachon, N. Mangold, O. Forni, L. C. Kah, A. Cousin, R. C. Wiens, R. Anderson, D. Blaney, J. G. Blank, F. Calef, S. M. Clegg, C. Fabre, M. R. Fisk, O. Gasnault, J. P. Grotzinger, R. Kronyak, N. L. Lanza, J. Lasue, L. L. Deit, S. L. Mouélic, S. Maurice, P.-Y. Meslin, D. Z. Oehler, V. Payré, W. Rapin, S. Schröder, K. Stack, D. Sumner, Chemistry of diagenetic features analyzed by ChemCam at Pahrump Hills, Gale crater, Mars. *Icarus* **281**, 121–136 (2017). doi:10.1016/j.icarus.2016.08.026

38. R. C. Anderson, L. Jandura, A. B. Okon, D. Sunshine, C. Roumeliotis, L. W. Beegle, J. Hurowitz, B. Kennedy, D. Limonadi, S. McCloskey, M. Robinson, C. Seybold, K. Brown, Collecting samples in Gale crater, Mars; an overview of the Mars science laboratory sample acquisition, sample processing and handling system. *Space Sci. Rev.* **170**, 57–75 (2012). doi:10.1007/s11214-012-9898-9

39. L. A. Leshin, P. R. Mahaffy, C. R. Webster, M. Cabane, P. Coll, P. G. Conrad, P. D. Archer Jr., S. K. Atreya, A. E. Brunner, A. Buch, J. L. Eigenbrode, G. J. Flesch, H. B. Franz, C. Freissinet, D. P. Glavin, A. C. McAdam, K. E. Miller, D. W. Ming, R. V. Morris, R. Navarro-González, P. B. Niles, T. Owen, R. O. Pepin, S. Squyres, A. Steele, J. C. Stern, R. E. Summons, D. Y. Sumner, B. Sutter, C. Szopa, S. Teinturier, M. G. Trainer, J. J. Wray, J. P. Grotzinger, MSL Science Team, Volatile, isotope, and organic analysis of martian fines with the Mars Curiosity rover. *Science* **341**, 1238937 (2013). doi:10.1126/science.1238937 Medline

40. D. P. Glavin, C. Freissinet, K. E. Miller, J. L. Eigenbrode, A. E. Brunner, A. Buch, B. Sutter, P. D. Archer Jr., S. K. Atreya, W. B. Brinckerhoff, M. Cabane, P. Coll, P. G. Conrad, D. Coscia, J. P. Dworkin, H. B. Franz, J. P. Grotzinger, L. A. Leshin, M. G. Martin, C. McKay, D. W. Ming, R. Navarro-González, A. Pavlov, A. Steele, R. E. Summons, C. Szopa, S. Teinturier, P. R. Mahaffy, Evidence for perchlorates and the origin of chlorinated hydrocarbons detected by SAM at the Rocknest aeolian deposit in Gale Crater. *J. Geophys. Res. Planets* **118**, 1955–1973 (2013). doi:10.1002/jgre.20144

41. D. R. Knapp, *Handbook of Analytical Derivatization Reactions* (Wiley-Interscience, 1979).

42. F. Stalport, D. P. Glavin, J. L. Eigenbrode, D. Bish, D. Blake, P. Coll, C. Szopa, A. Buch, A. McAdam, J. P. Dworkin, P. R. Mahaffy, The influence of mineralogy on recovering organic acids from Mars analogue materials using the "one-pot" derivatization experiment on the Sample Analysis at Mars (SAM) instrument suite. *Planet. Space Sci.* **67**, 1–13 (2012). doi:10.1016/j.pss.2012.02.010

43. P. D. Archer Jr., H. B. Franz, B. Sutter, R. D. Arevalo Jr., P. Coll, J. L. Eigenbrode, D. P. Glavin, J. J. Jones, L. A. Leshin, P. R. Mahaffy, A. C. McAdam, C. P. McKay, D. W. Ming, R. V. Morris, R. Navarro-González, P. B. Niles, A. Pavlov, S. W. Squyres, J. C. Stern, A. Steele, J. J. Wray, Abundances and implications of volatile-bearing species from evolved gas analysis of the Rocknest aeolian deposit, Gale Crater, Mars. *J. Geophys. Res. Planets* **119**, 237–254 (2014). doi:10.1002/2013JE004493

44. J. C. Stern, B. Sutter, C. Freissinet, R. Navarro-González, C. P. McKay, P. D. Archer Jr., A. Buch, A. E. Brunner, P. Coll, J. L. Eigenbrode, A. G. Fairen, H. B. Franz, D. P. Glavin, S. Kashyap, A. C. McAdam, D. W. Ming, A. Steele, C. Szopa, J. J. Wray, F. J. Martín-Torres, M.-P. Zorzano, P. G. Conrad, P. R. Mahaffy, MSL Science Team, Evidence for indigenous nitrogen in sedimentary and aeolian deposits from the Curiosity rover investigations at Gale crater, Mars. *Proc. Natl. Acad. Sci. U.S.A.* **112**, 4245–4250 (2015). doi:10.1073/pnas.1420932112 Medline

45. J. L. Eigenbrode, A. McAdam, H. Franz, C. Freissient, H. Bower, M. Floyd, P. Conrad, P. R. Mahaffy, J. Feldman, J. A. Hurowitz, J. Evans, M. S. Anderson, L. Jandura, K. Brown, C. Logan, S. Kuhn, R. Anderson, L. W. Beegle, D. Limonadi, R. Rainen, J. Umland, "Fluorocarbon contamination from the drill on the Mars Science Laboratory: Potential science impact on detecting martian organics by Sample at Mars (SAM)," paper presented at the 44th Lunar and Planetary Science Conference, Houston, TX, 18 to 22 March 2013.

46. F. Li, Z. Wu, Z. Shen, K. Chuang, R. E. Lyon, F. W. Harris, S. Z. D. Cheng, "The thermal and mechanical properties of high performance polyimide fibers," paper presented at the International Fire and Cabin Safety Research Conference, Atlantic City, NJ, 16 to 20 November 1998; https://www.fire.tc.faa.gov/1998Conference/presentations/StephenCheng.pdf (1998).

47. K. E. Miller, B. Kotrc, R. E. Summons, I. Belmahdi, A. Buch, J. L. Eigenbrode, C. Freissinet, D. P. Glavin, C. Szopa, Evaluation of the Tenax trap in the Sample Analysis at Mars instrument suite on the Curiosity rover as a potential hydrocarbon source for chlorinated organics detected in Gale Crater. *J. Geophys. Res. Planets* **120**, 1446–1459 (2015). doi:10.1002/2015JE004825

48. Y.-K. Kim, K. K. Irikura, M. E. Rudd, M. A. Ali, P. M. Stone, J. Chang, J. S. Coursey, R. A. Dragoset, A. R. Kishore, K. J. Olsen, A. M. Sansonetti, G. G. Wiersma, D. S. Zucker, M. A. Zucker, Electron-Impact Cross Sections for Ionization and Excitation Database, version 3.0 (National Institute of Standards and Technology, 2004); https://www.nist.gov/pml/electron-impact-cross-sections-ionization-and-excitation-database.

49. H. B. Franz, "Calibration constants for calculation of volatile abundances from Sample Analysis at Mars (SAM) evolved gas analysis (EGA) data" (TM-2017-217552, NASA, 2017).

50. T. Shin, O. Chuichi, W. Hajima, *Pyrolysis—GC/MS Data Book of Synthetic Polymers* (Elsevier, 2011).

51. P. G. Conrad, J. L. Eigenbrode, M. O. Von der Heydt, C. T. Mogensen, J. Canham, D. N. Harpold, J. Johnson, T. Errigo, D. P. Glavin, P. R. Mahaffy, The Mars Science Laboratory organic check material. *Space Sci. Rev.* **170**, 479–501 (2012). doi:10.1007/s11214-012-9893-1

52. H. Arito, R. Soda, Pyrolysis products of polytetrafluoroethylene and polyfluoroethylenepropylene with reference to inhalation toxicity. *Ann. Occup. Hyg.* **20**, 247–255 (1977). Medline

53. H. Busemann, A. F. Young, C. M. Alexander, P. Hoppe, S. Mukhopadhyay, L. R. Nittler, Interstellar chemistry recorded in organic matter from primitive meteorites. *Science* **312**, 727–730 (2006). doi:10.1126/science.1123878 Medline

54. M. A. Sephton, Pyrolysis and mass spectrometry studies of meteoritic organic matter. *Mass Spectrom. Rev.* **31**, 560–569 (2012). doi:10.1002/mas.20354 Medline

55. J. M. Hayes, Organic constituents of meteorites—a review. *Geochim. Cosmochim. Acta* **31**, 1395–1440 (1967). doi:10.1016/0016-7037(67)90019-1

56. C. Tian, C. R. Vidal, Electron impact dissociative ionization of CO_2: Measurements with a focusing time-of-flight mass spectrometer. *J. Chem. Phys.* **108**, 927–936 (1998). doi:10.1063/1.475456

57. K. K. Irikura, Semi-empirical estimation of ion-specific cross sections in electron ionization of molecules. *J. Chem. Phys.* **145**, 224102 (2016). doi:10.1063/1.4971242 Medline

58. V. Grill, G. Walder, D. Margreiter, T. Rauth, H. U. Poll, P. Scheier, T. D. Märk Absolute partial and total electron impact ionization cross sections for C_3H_8 from threshold up to 950 eV. *Z. Phys. D* **25**, 217–226 (1993). doi:10.1007/BF01426883